UNIVERSITY OF CALIFORNIA SAN DIEGO

K/Ka-Band Receive/Transmit Silicon Planar Phased Arrays for SATCOM

A dissertation submitted in partial satisfaction of the
requirements for the degree
Doctor of Philosophy

in

Electrical Engineering (Electronic Circuits and Systems)

by

Kevin Kai Wei Low

Committee in charge:

Professor Gabriel M. Rebeiz, Chair
Professor Gert Cauwenberghs
Professor William Hodgkiss
Professor Vitaliy Lomakin
Professor Daniel Sievenpiper

2021

Copyright
Kevin Kai Wei Low, 2021
All rights reserved.

The dissertation of Kevin Kai Wei Low is approved, and it is acceptable in quality and form for publication on microfilm and electronically.

University of California San Diego

2021

DEDICATION

To my beloved family and friends

EPIGRAPH

The way to get started is to quit talking and begin doing.

–Walt Disney

TABLE OF CONTENTS

LIST OF FIGURES

LIST OF TABLES

ACKNOWLEDGEMENTS

I would first like to thank my advisor, Professor Gabriel M. Rebeiz, for his invaluable expertise, mentorship and support during my doctoral studies. I first met the professor in 2015 at the International Microwave Symposium (IMS) in Phoenix, Arizona, when he was conducting a workshop on microwave tunable filters. I remember his passion and flair during that session that I thought it would be great if I could attend his classes as a student. Fate works in mysterious ways, and his former graduate student, who was my colleague at work, and would introduce me to Professor Rebeiz. A series of fortunate events happened and I was accepted as a Ph.D. student under his tutelage and support. Professor Rebeiz was strict and, under his supervision, we pushed and challenged the limits of research. It was tough but we learned a lot of things. He did not gave up on me when I was facing personal issues and aided me during periods of time when I was about to throw in the towel. He genuinely cares for his students and we are fortunate to have him as our advisor.

I would like to thank my ex-colleague, Kevin Ho, from Singapore. When he learned that I was considering graduate studies, introduced me to Professor Rebeiz and recommended me to him. Kevin would often talk about his experiences at UCSD and how he loved his student days in San Diego. This has definitely spurred my interest in pursuing a PhD track at UCSD. Without his encouragement and support, I would have never started on this graduate journey and I would not here today. I wish the best for Kevin and his family in Singapore.

I would like to thank my dissertation committee members, Prof. Gert Cauwenberghs, Prof. William Hodgkiss, Prof. Vitaliy Lomakin and Prof. Daniel Sievenpiper for their time, interest, and valuable comments about my research studies.

I would like to thank Ahmed Nafe for his mentorship and friendship. He has helped me a lot in various ways and is truly a person who can be depended upon. I would also like to thank Gokhan Gultepe for his mentorship and friendship. He entered the group with a lot of experience in phased-arrays and we've learned a lot of things from him. We had a lot conversations on the

difference between our countries like the culture and food. It was an eye-opener and definitely the second best take-away of the overseas PhD experience.

I would like to thank the rest of the Antenna team with special mentions of Bhaskara, Yusheng, Tom Phelps, Zhang Zhe, Sufan and Linjie. Thanks for the help, support and friendship. I would also like to thank the rest of TICSG especially Abdulrahman and Tsu-Wei for their support.

Lastly to my family and friends, thank you for your encouragement during this journey. I hope to meet up and chat away once we are able to. To my parents, thank you for your understanding and I can't wait to see you soon again.

This dissertation was completed with the generous support of Facebook, Renesas Electronics America (formerly IDT), and Qualcomm. I would also like to thank UCSD, for the graduate fellowship, Ansys and Keysight, for their design and simulation software, Keysight and ETS-Lindgren, for their measurement equipment, and Kyocera International, San Diego, for phased-array assembly.

The material in this dissertation is based on the following papers which are either published, has been submitted for publication, or contains material that is currently being prepared for submission for publication.

Chapter 2, in part, is a reprint of the material as it appears in: K. K. Wei Low, A. Nafe, S. Zihir, T. Kanar and G. M. Rebeiz, "A Scalable Circularly-Polarized 256-Element Ka-Band Phased-Array SATCOM Transmitter with ±60° Beam Scanning and 34.5 dBW EIRP," *2019 IEEE/MTT-S International Microwave Symposium (IMS)*, Boston, MA, USA, 2019, pp. 1064-1067, doi: 10.1109/MWSYM.2019.8701112. The dissertation author was the primary investigator and author of this paper.

Chapter 3, in part, is a reprint of the material as it appears in: K. K. Wei Low, S. Zihir, T. Kanar and G. M. Rebeiz, "A Scalable Switchable Dual-Polarized 256-Element Ka-Band SATCOM Transmit Phased-Array with Embedded RF Driver and ±70° Beam Scanning," *2020 IEEE/MTT-S*

International Microwave Symposium (IMS), Los Angeles, CA, USA, 2020, pp. 821-824, doi: 10.1109/IMS30576.2020.9223891. The dissertation author was the primary investigator and author of this paper.

Chapter 4, in part, is a reprint of the material as it appears in: K. K. Wei Low, S. Zihir, T. Kanar and G. M. Rebeiz, "A Reconfigurable Dual-Polarized 1024-Element Ka-Band SATCOM Transmit Phased-Array with Large Scan Volume and +48 dBW EIRP," presented at 2021 IEEE/MTT-S International Microwave Symposium (IMS), Atlanta, GA, USA, Jun. 10, 2021. The dissertation author was the primary investigator and author of this paper.

Chapter 4 is also, in full, has been submitted for publication of the material as it may appear in: K. K. Wei Low, S. Zihir, T. Kanar and G. M. Rebeiz, "A 27-31 GHz 1024-Element Ka-Band SATCOM Phased-Array Transmitter with 49.5-dBW Peak EIRP, 1-dB AR, and ±70° Beam Scanning," in *IEEE Transactions on Microwave Theory and Techniques*, submitted. The dissertation author was the primary investigator and author of this paper.

Chapter 5, in full, has been submitted for publication of the material as it may appear in: K. K. Wei Low, T. Kanar, S. Zihir and G. M. Rebeiz, "A 17.7-20.2 GHz 1024-Element K-Band SATCOM Phased-Array Receiver with 8.1 dB/K G/T, ±70° Beam Scanning, and High Transmit Isolation," in *IEEE Transactions on Microwave Theory and Techniques*, submitted. The dissertation author was the primary investigator and author of this paper.

VITA

2013	Bachelor of Engineering in Electrical Engineering, National University of Singapore, Singapore
2013-2017	Member of Technical Staff, DSO National Laboratories, Singapore
2020	Master of Science in Electrical Engineering (Electronic Circuits and Systems), University of California San Diego, USA
2021	Doctor of Philosophy in Electrical Engineering (Electronic Circuits and Systems), University of California San Diego, USA

PUBLICATIONS

K. K. Wei Low, T. Kanar, S. Zihir and G. M. Rebeiz, "A 17.7-20.2 GHz 1024-Element K-Band SATCOM Phased-Array Receiver with 8.1 dB/K G/T, ±70° Beam Scanning, and High Transmit Isolation," in *IEEE Transactions on Microwave Theory and Techniques* (submitted).

K. K. Wei Low, S. Zihir, T. Kanar and G. M. Rebeiz, "A 27-31 GHz 1024-Element Ka-Band SATCOM Phased-Array Transmitter with 49.5-dBW Peak EIRP, 1-dB AR, and ±70° Beam Scanning," in *IEEE Transactions on Microwave Theory and Techniques* (submitted).

K. K. Wei Low, S. Zihir, T. Kanar and G. M. Rebeiz, "A Reconfigurable Dual-Polarized 1024-Element Ka-Band SATCOM Transmit Phased-Array with Large Scan Volume and +48 dBW EIRP," presented at 2021 IEEE/MTT-S International Microwave Symposium (IMS), Atlanta, GA, USA, Jun. 10, 2021.

K. K. Wei Low, S. Zihir, T. Kanar and G. M. Rebeiz, "A Scalable Switchable Dual-Polarized 256-Element Ka-Band SATCOM Transmit Phased-Array with Embedded RF Driver and ±70° Beam Scanning," *2020 IEEE/MTT-S International Microwave Symposium (IMS)*, Los Angeles, CA, USA, 2020, pp. 821-824, doi: 10.1109/IMS30576.2020.9223891.

K. K. Wei Low, A. Nafe, S. Zihir, T. Kanar and G. M. Rebeiz, "A Scalable Circularly-Polarized 256-Element Ka-Band Phased-Array SATCOM Transmitter with ±60° Beam Scanning and 34.5 dBW EIRP," *2019 IEEE/MTT-S International Microwave Symposium (IMS)*, Boston, MA, USA, 2019, pp. 1064-1067, doi: 10.1109/MWSYM.2019.8701112.

T. Lin, K. K. Wei Low, R. Gaddi and G. M. Rebeiz, "High-Linearity 5.3-7.0 GHz 3-Pole Tunable Bandpass Filter Using Commercial RF MEMS Capacitors," *2018 48th European Microwave Conference (EuMC)*, 2018, pp. 555-558, doi: 10.23919/EuMC.2018.8541669.

ABSTRACT OF THE DISSERTATION

K/Ka-Band Receive/Transmit Silicon Planar Phased Arrays for SATCOM

by

Kevin Kai Wei Low

Doctor of Philosophy in Electrical Engineering (Electronic Circuits and Systems)

University of California San Diego, 2021

Professor Gabriel M. Rebeiz, Chair

This dissertation focuses on building state-of-the-art planar, all-silicon active electronically scanned array (AESA) for satellite communications (SATCOM) ground terminals and SATCOM on-the-move (SOTM) terminals, as well as emerging non geosynchronous orbits (GEO) SATCOM systems. Three Ka-band phased-arrays transmitters (a 256-element array capable of 1-D scan, a 256-element array capable of 2-D scan, and a 1024-element array capable of 2-D scan) and one K-band phased-array receiver (1024-element) are presented. The planar phased-arrays integrate commercially available silicon beamformer chips, silicon low noise amplifier (LNA) chips, printed Wilkinson divider/combiner beamforming network (BFN), and printed planar dual-polarized patch antennas on a single printed circuit board (PCB) and represent the highest

level of integration at millimeter-waves. The 1024-element phased-arrays, in particular, have record results in published effective isotropic radiated power (EIRP) and gain to noise temperature (G/T) for K/Ka-band planar phased-arrays for SATCOM applications.

Chapter 1

Introduction

Since inception and first demonstrated in 1905 by Nobel laureate Karl F. Braun, phased-arrays have almost always exclusively been used in defense and high-value SATCOM on-the-move (SOTM) systems due to their high cost. Modern AESA have come a long way since then and now they are generally built using custom hand-tuned transmit/receive (T/R) modules, and assembled together, individually by hand with antennas to build a large thousand-element phased-array. Even higher integration has historically been hampered by the ability to integrate functionalities of a T/R module onto a single chip.

However, with recent advances in silicon technology, single chip multi-channel beamformers (BF) are now commercially available with low power and high performance approaching capabilities of those custom GaAs T/R modules. Each multi-channel beamformers can take the place of multiple GaAs T/R modules and be integrated with antennas directly on a single PCB. This new take on AESA integration will reduce manual assembly, improve yield, reduce length of the design cycle, and hence reduce cost to develop a phased-array product. And over time, due to process maturity and economy of scale, the cost of silicon beamformer chips will be lowered as well. All this would mean that it would be feasible for user terminals to be outfitted with these advanced AESA at relatively low cost in the near future. In fact, with proper business model and

(a)

(b)

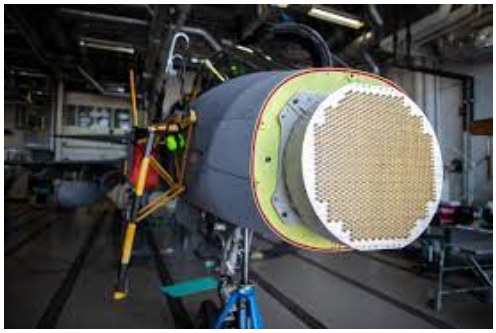

(c)

Figure 1.1: Examples of modern AESA on (a) marine, (b) land, and (c) airbone military platforms. Image credits : IAI Elta, Raytheon, Saab, Wikipedia.

subsidy, low cost AESA user terminal has been available to customers of at least one emerging SATCOM service provider.

1.1 The Need for AESA User Terminals

In recent years, demand for increase in capacity and reduction in latency using satellite communication (SATCOM) has shifted focus of its operation to use of the lower medium earth orbit (MEO) and low earth orbit (LEO) instead of the traditional geosynchronous orbit (GEO). The push to lower orbits has presented a new challenge for user ground terminals which is currently dominated by use of large relatively inexpensive reflector-based antennas which do not have the capability to scan. The new requirement of these terminals to scan/track the satellites (on

the lower orbit), as they move across the sky, necessitates complex mechanical scanning units and the cost and long-term reliability of these upgrades are not negligible. An ideal solution would be to use AESA and adoption will require it to be cost competitive to the large mechanical scanning unit. Integrating silicon beamformers and antennas onto a single PCB reduces labor and hence cost of AESA. Cost of these AESA will also benefit from economy of scale as users increase. Affordable phased-arrays also benefit current GEO SATCOM systems and SOTM systems.

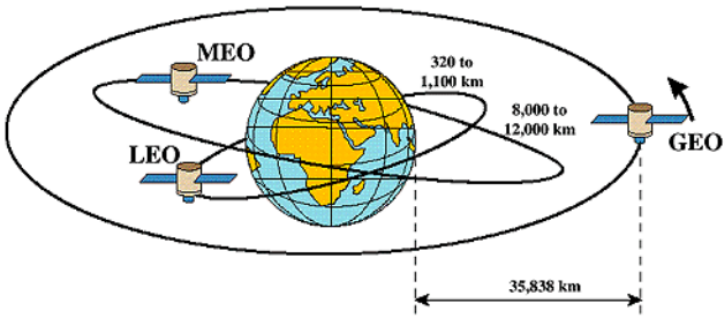

Figure 1.2: Pictogram depicting the different commonly used SATCOM satellite orbits. Image credit : IEEE.

1.2 State of Commercial SATCOM User Terminals

With current SATCOM systems still deploying satellites on GEO, the commerical user ground terminal is dominated by large reflector based antennas because of cost. Without the need for scanning, there is little incentive to develop an antenna with electronic beam steering such as AESA which can be costly. The technology and know-hows of reflector antennas are very mature and modules to build it can be bought off the shelves. This has led to inexpensive large scale manufacturing and roll-out of these antennas.

Even for GEO-based systems, there exist a small market for antennas which can scan. These are SATCOM antennas mounted on a ship, plane, and ground vehicles that require constant satellite connection. The commercial development of scanning antennas has largely led to

(a) (b)

(c)

Figure 1.3: (a) A 1.8 m SATCOM Ku-band user ground terminal. (b) Ku-band SATCOM user marine terminal mounted on a mechanical scanning unit. (c) X-band slotted waveguide mast mounted radar on a ship. Image credits : VSAT, Cobham, Wikipedia.

use of mechanical assistance to support some degree of beam steering required since reflector based antennas are cost effective and well-understood. These are usually a reflector mounted on a complex mechanical scanning unit with motors supporting 2-D steering of the antenna. These are usually quite bulky and even the smallest ones are not low-profile. The size, weight, and large-profile means that it is usually used for ground based SOTM terminals or on ships. For mounting on planes, there is an antenna made by ThinKom designed specially to have a low-profile and support 2-D scan as well. By passing the beam through a set of two rotating discs, they were able to steer the beam while remaining low-profile. These two solution can be expensive to build since integration with mechanical steering can be labor intensive.

Currently, these solutions for mechanical scanning can be costly or bulky, limiting them to

large high-value platforms. With the advancement of silicon planar AESA technology, the cost of planar phased-arrays are becoming affordable. This has happened with Ku-band SATCOM where subsidy and marketing strategy has pushed affordable AESA to the hands of consumers. This will push research and development of higher bandwidth SATCOM systems such as Ka-band in the future and demand for it might justify an upgrade to Ka-band for higher speeds.

1.3 Thesis Overview

This thesis presents the design and analysis of affordable, planar low-profile, high performance K/Ka-band SATCOM AESAs and demonstrates the performance of these phased-arrays and compares them with the state-of-the-art.

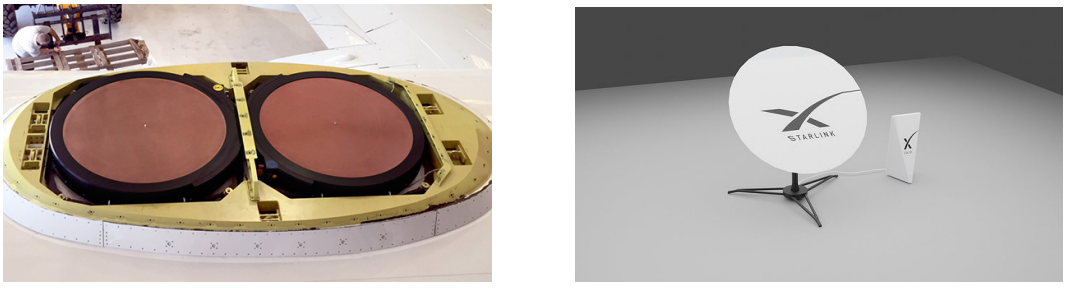

(a) (b)

Figure 1.4: (a) Low profile SATCOM terminal for planes bridges gap between reflectors and AESA. (b) Next-generation 0.6 m AESA SATCOM user ground terminal for Ku-band. Image credits : ThinKom, Starlink.

Chapter 2 presents a scalable 256-element Ka-band switchable dual-polarizrd phased-array SATCOM transmitter (TX). The phased-array can generate linear, rotated linear, clockwise and counter-clockwise polarization which can be selected by setting the phased shifters in the beamformer chips. The low-cost design uses FR-4 based printed circuit board (PCB), surface mount technology (SMT) and silicon beamformer chips. The phased-array can scan to ±60° in the elevation plane with a 3-dB beamwidth of 7° and 34.5 dBW EIRP at broadside. It has a measured 3-dB instantaneous axial-ratio bandwidth of 2 GHz and is scalable without grating lobes to allow

economical construction of larger phased-arrays. The compact size of (14 cm x 11.5 cm) makes it suitable for a low-cost Ka-band SATCOM terminal.

Chapter 3 presents a scalable switchable dual-polarized 256-element Ka-band SATCOM transmit (TX) phased-array with embedded driver. The phased-array is based on 64 SiGe 8-channel TX beamformer chips and uses low-cost printed circuit board (PCB) and surface mount technology (SMT). The phased-array can transmit clockwise and counter-clockwise polarization which is suitable for Ka-band SATCOM. It demonstrates a measured 6.8° 3-dB beamwidth, +32 dBW (+62 dBm) EIRP on axis, greater than 25 dB cross-polar discrimination (XPD) and the ability to scan to ±70° in all planes. The scalable nature allows for economical construction of larger phased-array without grating lobes. A compact size of 11.7 cm x 7.5 cm makes it suitable for Ka-band SATCOM portable terminals.

Chapter 4 presents a wideband scalable 27-31 GHz 1024-element Ka-band SATCOM transmit (TX) phased-array with embedded RF drivers and reconfigurable polarization. The phased-array uses silicon TX beamformer (BF) chips and printed stacked-patch antennas on a FR-4 based printed circuit board (PCB) to transmit either linear, rotated linear, circular clockwise or anticlockwise polarization. It demonstrates a measured 3.5° half-power beamwidth (HPBW), 35 dB cross-polar discrimination (XPD), sub 1 dB axial ratio (AR), +49.5 dBW peak effective isotropic radiated power (EIRP) on axis and the ability to scan to ±70° in all planes without grating lobes and $cos^{1-1.1}(\theta)$ scan loss. Measured error vector magnitude (EVM) of less than 2.3% and adjacent channel power ratio (ACPR) of less than -32 dBc across all scan at P_{1dB} makes it suitable as a compact high efficiency SATCOM transmitter. The array aperture measures 14.9 cm by 14.9 cm and it is scalable to larger phased-arrays with 4096 and higher number of elements. To our knowledge, this represents the highest level of integration at millimeter-waves, and with the highest measured EIRP from a SATCOM phased-array.

Chapter 5 presents a wideband scalable 17.7-20.2 GHz 1024-element K-band SATCOM receive (RX) phased-array with reconfigurable polarization. The phased-array uses silicon RX

beamformer (BF) chips and silicon low noise amplifiers (LNA) and is able to receive either linear, rotated linear, circular clockwise or anticlockwise polarization. It demonstrates a measured 3.47° half-power beamwidth (HPBW), more than 25 dB cross-polar discrimination (XPD), +8.1 dB/K gain to noise (G/T) per polarization, and has more than 80 dB Tx-band isolation. The phased-array is able to scan to $\pm 70°$ in all planes without grating lobes and $cos^{1-1.2}(\theta)$ scan loss. The array aperture measures 22.4 cm by 22.4 cm. To our knowledge, this is the largest SATCOM K-band phased-array to-date with the highest G/T and represents the highest level of integration at millimeter-waves.

Chapter 6 concludes the dissertation and discusses future work.

Chapter 2

A Scalable Circularly-Polarized 256-Element Ka-Band Phased-Array SATCOM Transmitter with ±60° Beam Scanning and 34.5 dBW EIRP

2.1 Introduction

The new wave of SATCOM broadband is set to challenge cable and mobile for telecommunication and internet access in low density areas (poorly served areas) [1]. Users increasingly demand better coverage around the world at similar speeds as mobile broadband, and Ka-band SATCOM has the bandwidth and multi-beam capabilities to provide such a service. Also, for users on a plane or a ship (mobile), SATCOM is the only solution available but it is hampered by relatively high-cost mechanically-steered units requiring precise pointing accuracy [2]–[3].

Traditional SATCOM broadband operates using geostationary (GEO) satellites which

require large ground terminals, but newly proposed constellations in low and medium Earth orbit (LEO and MEO) is set to change that. Unlike GEO, LEO and MEO-based broadband promises higher speed, lower latency and greater coverage. Also operating broadband SATCOM at LEO and MEO relaxes the link requirement and leads to smaller and less expensive satellite user equipment [4].

LEO and MEO-based satellites require that ground equipment (single user terminals or internet service providers) track the satellite as it orbits around the earth. This necessitates either complex mechanical scanning units or electronically scanned phased-arrays [4].

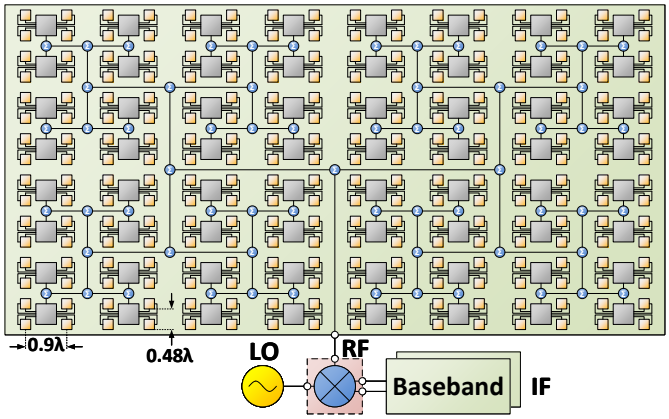

Figure 2.1: A 256-element dual-polarized phased-array Ka-band SATCOM transmitter based on 64 8-channel beamformer chips. The phased-array can generate linear, rotated linear, clockwise and counter-clockwise polarization by setting the phase shifters in the 8-channel beamformer chips.

The aim of this work is to demonstrate a low-cost scalable circularly-polarized Ka-band transmit phased-array capable of ±60° scanning in one plane using 256-elements. The phased-array architecture employed is similar to [5]–[6] and is shown in Fig. 2.1. The design approach employs printed circuit board (PCB), surface mount technology (SMT) and silicon beamformer core chip architecture [7]–[8] to enable a low-cost Ka-Band SATCOM transmit solution with high economy of scale.

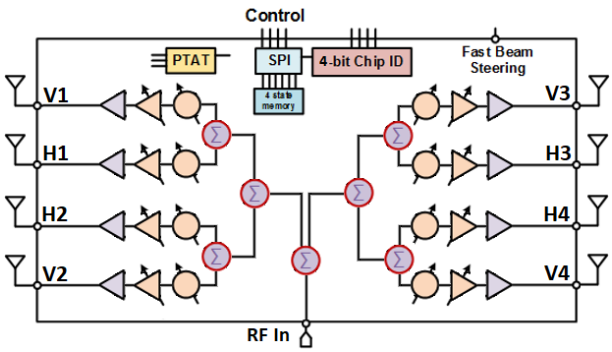

Figure 2.2: Block diagram of the 8-channel Ka-band transmit beamformer chip.

2.2 Silicon 8-Channel TX Beamformer

The transmit (Tx) beamformer flip-chip is based on a SiGe BiCMOS process and its block diagram is shown in Fig. 2.2. Each Ka-band beamformer contains 8 identical transmit channels each with a power amplifier, a variable gain amplifier with $>$ 20 dB gain control and a 6-bit phase shifter. The beamformer has a measured output P1dB of 7-8 dBm per channel, an electronic gain of 12 dB at 28-30 GHz and consumes about 0.9 W from a 2.3 V supply. Higher P1dB and EIRP can be obtained by adding external power amplifiers (not shown).

The beamformer gain, phase and built-in PTAT current bias can be controlled using a 4-wire serial-peripheral interface (SPI). It also has 4-bit hardware address allowing a simple way to share the SPI bus for up to 16 chips without multiple chip-select lines. The flip-chip package employs 0.4 mm pitch solder bumps. The wide pitch allows it to be assembled directly onto a PCB without an interposer allowing for high density packaging without sacrificing performance.

2.3 Ka-Band SATCOM TX Phased-Array Design

The 256-element Ka-Band SATCOM Tx phased-array is built on a low-cost FR-4 based multi-layer PCB with $\varepsilon_r = 3.26$ and $\tan\delta = 0.005$ at 30 GHz. The PCB stackup, Fig. 2.3, consisting of 12-layers has 1 set of plated-through hole (PTH) vias and 3 sets of blind vias (not shown).

The block diagram of the phased-array is shown in Fig. 2.1. A total of 64 beamformer

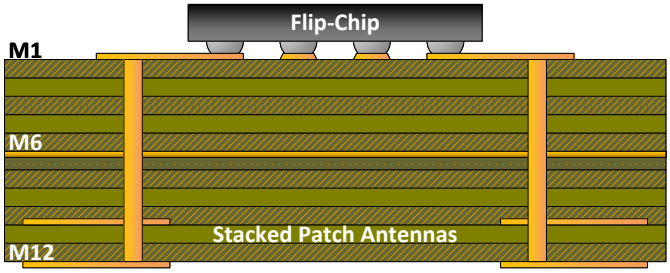

Figure 2.3: Low cost PCB stack-up for the Ka-band SATCOM transmitter.

chips are assembled on M1 with each chip controlling 4 dual-polarized antennas on M12. Grounded CPW transmission lines are used to connect the RF output ports to the antennas. Each of the 64 beamformer chips are fed by a 1:64 corporate divider implemented using 63 printed Wilkinson power divider and 100 Ω commercially available 0201 SMT resistors on M1. Note that external PAs were not used on this PCB, and therefore, this design has room for improvement on EIRP.

The dual-polarized antennas elements are designed on M10 with parasitic patches on M12 to achieve about 10% fractional bandwidth and 15 dB return loss (28-31 GHz). The antennas are probe-fed with a ground on M6, and contain two feeds, one for V-polarization and one for H-polarization, with an isolation of 17 dB between the feeds (not shown due to brevity). The phased-array is designed for ±60° scan in the elevation plane with high EIRP by arranging the elements on 8.75 mm x 4.67 mm grid (0.9λ x 0.48λ at 31 GHz). The antennas are also arranged in a sequentially rotated manner to reduce the cross-polarization levels generated by the probe feeds. Note that this design allows for only ±5° scanning in the azimuth plane and therefore requires a phi-rotated mechanical mount for azimuth scan.

A fully assembled 256-element Ka-band phased-array with an active area measuring 140 mm x 74.8 mm is shown in Fig. 2.4. The digital control and power delivery, embedded in inner layers M3 to M5, are split into 4 identical vertical columns each serving 16 beamformer chips with separate connectors. This approach improves yield and eliminate single point of failure. Selective removal of soldermask facilitates waste heat removal using heatsink. The phased-array

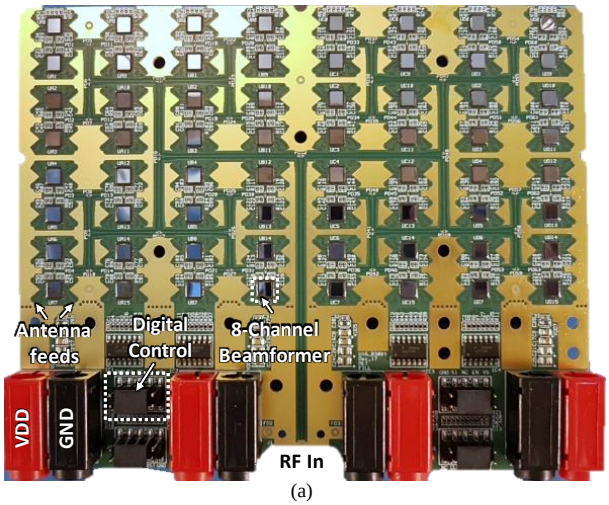

(a)

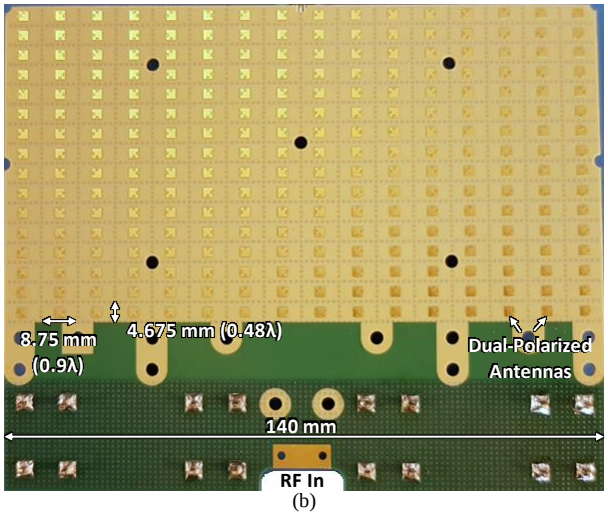

(b)

Figure 2.4: (a) Top view and (b) bottom view of the 256-element Ka-band phased-array SATCOM transmitter.

is scalable (2xN) without grating lobes, combining into a larger phased-array by placing more copies of it side-by-side, allowing for a cost-effective upgrade for this design approach.

2.4 Measurements

The phased-array was measured and calibrated in the far-field using a VNA and a receive standard gain horn at a range of R = 1.85 m (between D^2/λ and $2D^2/\lambda$), as seen in Fig. 2.5.

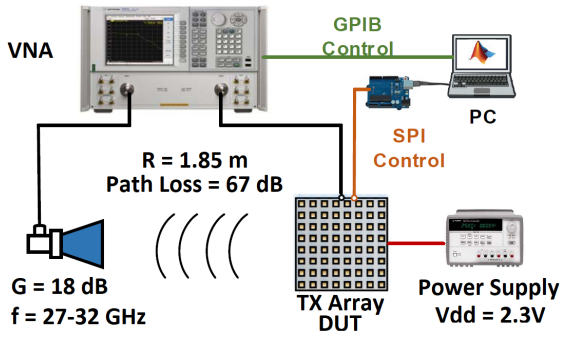

Figure 2.5: Far-field measurement setup.

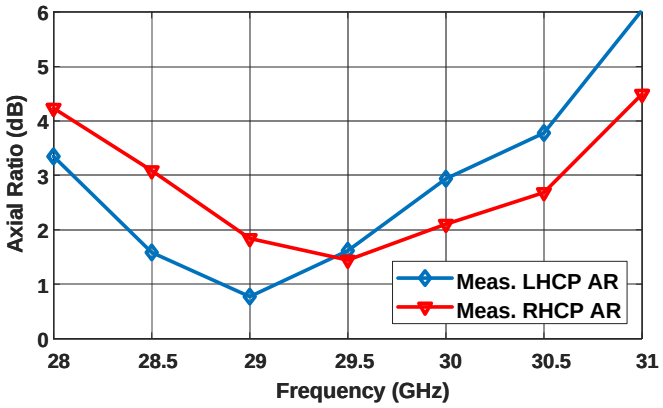

Figure 2.6: Measured axial ratio when phased-array is calibrated at 29.5 GHz.

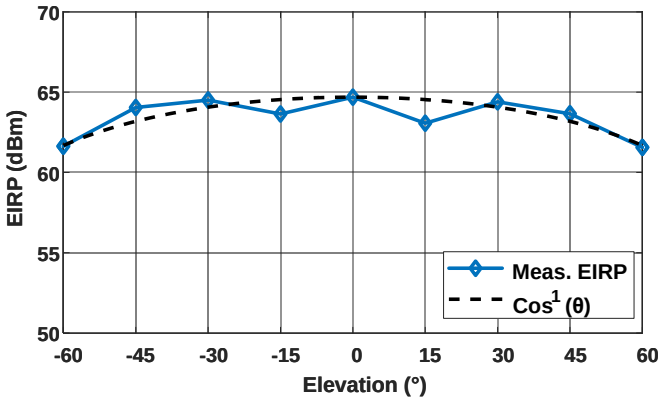

Figure 2.7: Measured LHCP EIRP of the 256-element phased-array at 29.5 GHz.

A simple calibration was done by measuring, at broadside, every element gain and phase in the lowest phase and highest gain state with all other elements turned off. The measurement was used to determine the gain and phase calibration required at every frequency using lookup

tables. Calibration at 29.5 GHz was then applied and the measured axial ratio, Fig. 2.6, shows 2 GHz of instantaneous 3-dB bandwidth for both LHCP and RHCP. Better axial ratio can be achieved by calibrating with every element turned on, using different calibration for different scan angles and using more calibration iterations.

Fig. 2.7 presents the measured LHCP EIRP at 29.5 GHz of the 256-element phased-array versus scan angle. The phased-array achieves an EIRP of 63.5 dBm at 1 dB compression and 64.5 dBm at saturation. This agrees well with the calculation of circularly-polarized EIRP given by:

$$\begin{aligned} EIRP_{-1dB,CP} &= 20log_{10}(N) + G_{ant} + P_{element,CP} \\ &= 60.2 + 3.5 + 10 = 64\,dBm \end{aligned} \tag{2.1}$$

where

$$G_{ant} = D_{ant} - loss = 6\,dB \tag{2.2}$$

and D (7.3 dB) is the Directivity of an antenna element in a 0.9λ x 0.48λ, and loss (1.3 dB) is the total antenna and transmission-line loss between the chip and the antennas. A P1dB of 10 dBm is taken since both channels are turned on for a circularly-polarized pattern.

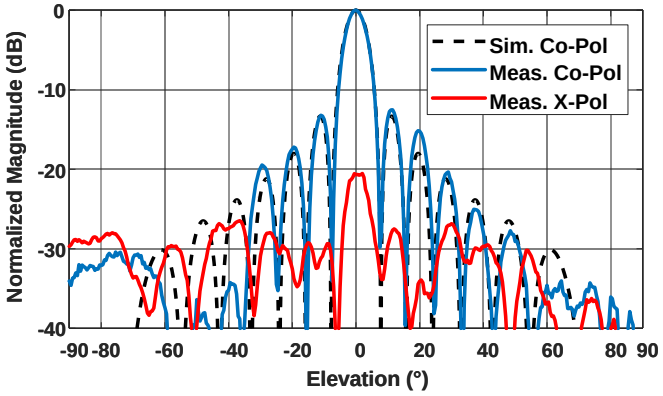

Figure 2.8: Measured LCHP co-and cross-polarization pattern scanned to broadside at 29.5 GHz with uniform illumination.

The measured LHCP co- and cross-polarization patterns, Fig. 2.8, shows < -21 dB cross-polarization and < -13 dB sidelobe levels for uniform illumination. The 3-dB beamwidth is 7° and 3.5° in the elevation and azimuth (not shown) plane and agrees very well with simulations. Sidelobes can be reduced to < -20 dB using an 8 dB cosine amplitude taper (not shown due to brevity).

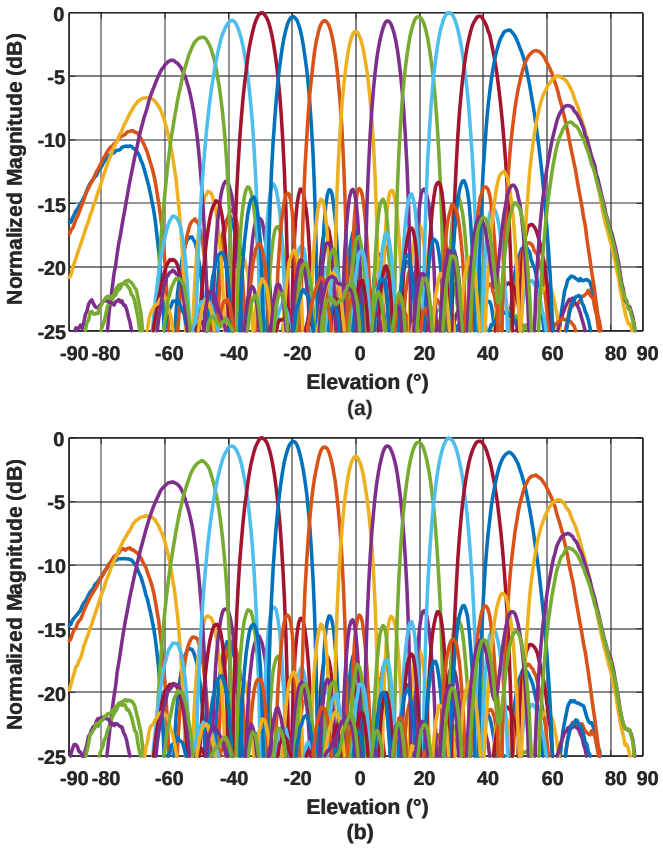

Figure 2.9: Measured scanned co-pol patterns at 29.5 GHz (a) LHCP, (b) RHCP.

Fig. 2.9 presents the measured LHCP and RHCP co-polarized patterns as the array scans in the elevation plane. The phased-array can scan to ±60° with 3.7 dB loss and up to ±70° (with higher loss) without grating lobes. The phased-array consumes 57.6 W (76 W at P1dB) from 2.3 V supply when operated in both V and H polarizations (circular polarization).

2.5 Conclusion

This paper presents a low cost, circularly-polarized 256-element phased-array SATCOM transmitter in the Ka-band with 34.5 dBW EIRP and can scan to ±60° in elevation and ±5° in azimuth. The narrow 7°/3.5° beamwidths in the elevation/azimuth planes allow it to be used for SATCOM systems utilizing LEO and MEO constellation. The design can be scaled economically in a 2xN configuration without grating lobes for higher EIRP.

2.6 Acknowledgment

The authors thank Integrated Device Technology, IDT, for sponsoring the beamformer chips used in this work. The array was assembled by Kyocera International, San Diego, using their advanced phased-array assembly line. Ka-band SATCOM beamformer chips (different versions) are available from IDT.

Chapter 2, in part, is a reprint of the material as it appears in: K. K. Wei Low, A. Nafe, S. Zihir, T. Kanar and G. M. Rebeiz, "A Scalable Circularly-Polarized 256-Element Ka-Band Phased-Array SATCOM Transmitter with ±60° Beam Scanning and 34.5 dBW EIRP," *2019 IEEE/MTT-S International Microwave Symposium (IMS)*, Boston, MA, USA, 2019, pp. 1064-1067, doi: 10.1109/MWSYM.2019.8701112. The dissertation author was the primary investigator and author of this paper.

Chapter 3

A Scalable Switchable Dual-Polarized 256-Element Ka-Band SATCOM Transmit Phased-Array with Embedded RF Driver and ±70° Beam Scanning

3.1 Introduction

Traditional SATCOM systems operate using geostationary (GEO) satellites which requires large ground terminals, but new constellations in low earth orbit (LEO) and medium-earth orbit (MEO) are set to change that [1]. Operating SATCOM in LEO and MEO relaxes the link budget leading to lower power requirement and ultimately smaller and less expensive satellite user equipment. One drawback of LEO/MEO systems is that they require ground equipment to track the satellite as it orbits around earth. This necessitates complex mechanical scanning unit which can be large or expensive. SATCOM is also the only solution for users on a plane or ship, but it has been hampered by the relatively high-cost mechanically-steered units requiring precise

pointing accuracy [9]. However, with recent advances in silicon-based phased-arrays, it has become possible to manufacture portable planar electronically-scanned phased-arrays, which can be used for either LEO/MEO systems, or for GEO SATCOM-on-the-move systems [10], [11], [5], [12].

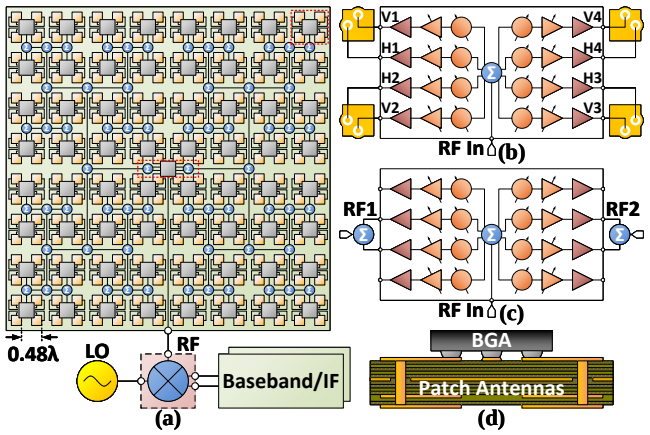

Figure 3.1: (a) Block diagram of 256-element dual-polarized SATCOM TX phased-array. (b) 8 channel TX beamformer block diagram. (c) Embedded TX driver. (d) Low-cost PCB stack-up.

In this paper, a planar scalable dual-polarized 256-element Ka-band SATCOM TX phased-array is demonstrated with full 2-D scanning. Previously, 1-D scan phased-array was demonstrated with a relaxed pitch in one axis [13]. This work expands on [5], [12], [13], [14], [15], and demonstrates the use of embedded drivers to lower the input power requirement of large phased-arrays (Fig. 3.1a).

3.2 Ka-Band SATCOM TX Phased-Array Design

3.2.1 Silicon 8-Channel TX Beamformer Chip

The TX beamformer BGA chip is designed in a SiGe BiCMOS process for Ka-band SATCOM phased-array applications (Fig. 3.1b). The core IC has 6-bit phase control coupled with more than 35 dB gain on each channel to achieve fine beam steering and gain compensation

between radiating elements. It has 25 dB nominal gain, 7-8 dBm output P1dB and achieves an RMS phase and gain error of 3° and 0.4 dB over the frequency of operation.

The beamformer gain, phase can be independently controlled using high-speed 4-wire serial-peripheral interface (SPI). The chip comes with hardware selectable address allowing for multiple chips on a single SPI bus. The ball grid array (BGA) package employs 0.5 mm ball pitch, measures 3.8 mm x 4.6 mm, and is easy to assemble in an automated assembly line.

3.2.2 Dual-Polarized Stacked-Patch Antenna Design

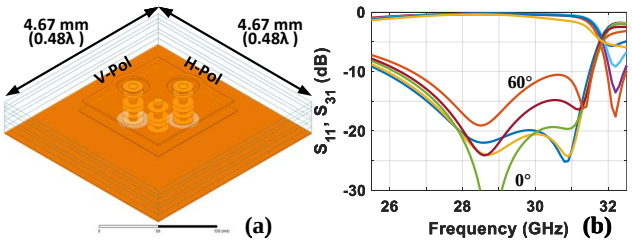

Figure 3.2: (a) Stacked patch antenna unit-cell and simulated (b) H-plane transmission and reflected coefficients over different scan angles.

The antenna element is a probe-fed dual-polarized stacked-square patch (Fig. 3.2a) on a low-cost FR-4 based multi-layer PCB (Fig. 3.1d) with $\varepsilon_r = 3.26$ and $\tan\delta = 0.005$ at 30 GHz. The antennas are placed in a square grid with a spacing of 4.67 mm (0.48λ at 31 GHz). It is polarization mirror symmetric; the performance of vertical-polarized element is identical to the horizontal-polarized element.

The simulated performance is shown in Fig. 3.2b (H-plane). The antennas are well matched with reflection coefficient S11 < -15 dB. The transmission coefficient S31 (includes ohmic and mismatch losses) remains > -1 dB on axis from 27-31 GHz. S11 remains < -10 dB and S31 remains > -3 dB as the array scans to ±60°. The simulated XPD is > 20 dB.

3.2.3 Digital Control And PCB Design

A fully assembled 256-element Ka-band phased-array with an active area measuring 74.7 mm x 74.7 mm is shown in Fig. 3.3. Full RF beamforming was employed for the design of the phased-array (Fig. 3.1a) with the addition of an embedded RF driver (Fig. 3.1c) to overcome ohmic losses in the distribution network. The 1:64 corporate divider network uses grounded co-planar waveguide (G-CPW) on M1 and commercially available 0201 SMT 100 Ω resistor.

An embedded RF driver (Fig. 3.1c) uses four channels of the beamformer and serves as a compact active power divider in place of the first divider in the distribution network. The high gain and linearity of the RF driver reduces the phased-array input power requirement to -10 dBm (at P1dB) without reducing linearity. Having RF drivers with phase and gain control also allows for calibration at the subarray level which is important when several 256-element arrays are combined to build a large phased-array. Also, using the RF driver for calibration in subarrays greatly reduces the variation between subarrays and preserves the gain dynamic range of individual channels.

High-speed digital line buffers were included for the digital control lines, and the phased-array is controlled using a low-cost commercially available ARM based microcontroller board. Layers M3 to M5 were used for digital control and power delivery, and the phased-array is scalable (2xN) allowing for a cost-effective upgrade for this design approach. The phased-array PCB measures 116.8 mm x 74.7 mm.

3.3 Calibration And Measurements

The phased-array was calibrated and measured in the ETS-Lindgren 5700 anechoic chamber using a vector network analyzer (VNA) and dual-polarized horn at range R = 1.06 m (phased-array $R_{far-field} = 2D^2/\lambda$ = 1.08 m at 29 GHz) as seen in Fig. 3.3c. Phi and theta motorized antenna-under-test (AUT) setup, available in the chamber, allows for full two dimension

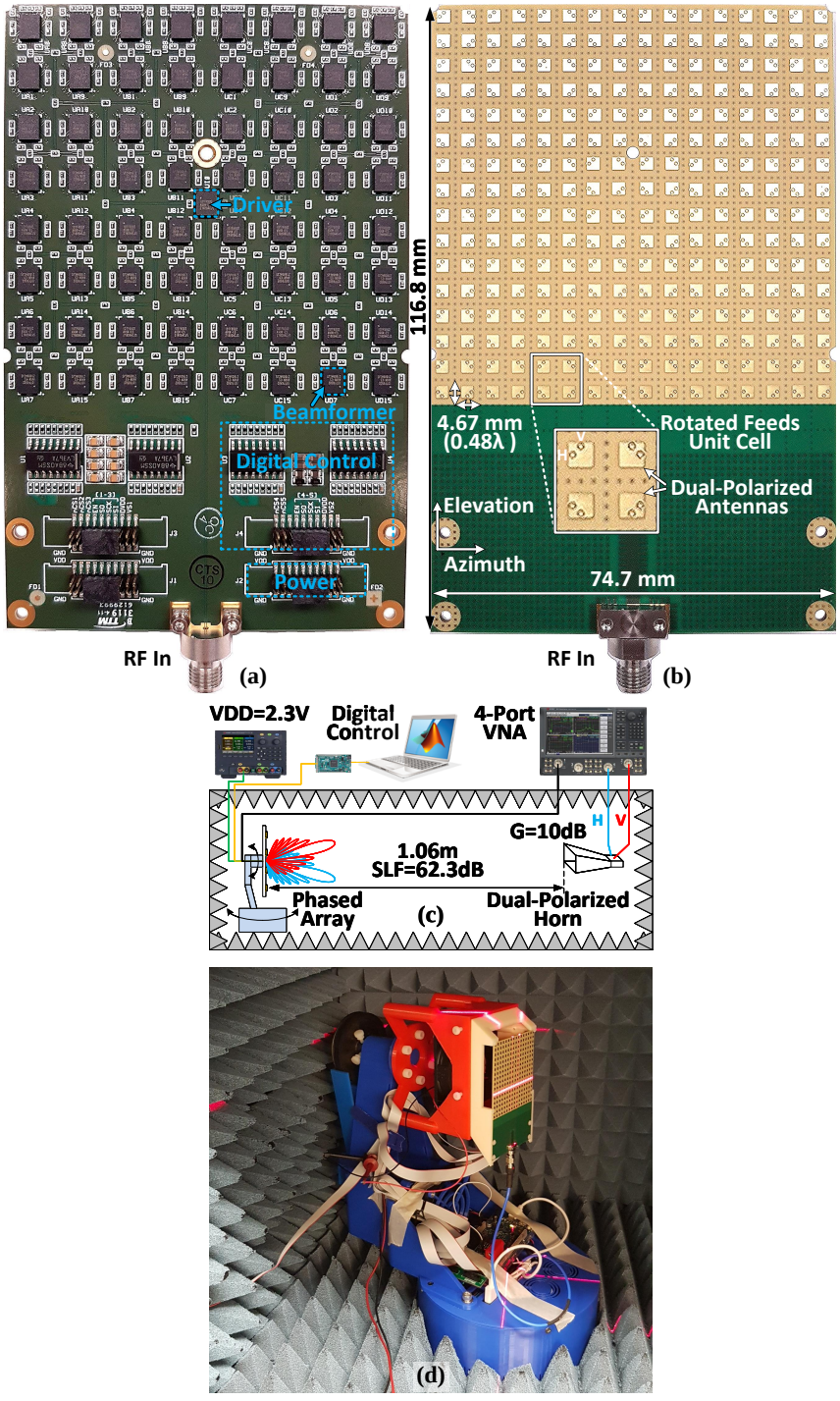

Figure 3.3: (a) Top view and (b) bottom view of the 256-element switchable dual-polarized Ka-band SATCOM TX phased-array (this work). Far-field measurement setup: (c) block diagram and (d) photograph of the phased-array affixed on a motorized phi-over-theta rotary mount.

(2-D) array pattern measurements (Fig. 3.3d).

Calibration was done, on axis, by measuring every element individually and correcting for the phase and amplitude error. The calibration process is iterative; it ends when desired RMS phase and gain errors were met or when it reaches the maximum iterations. This results in low RMS phase and gain errors of 3.3° and 0.4 dB, respectively, at 29 GHz.

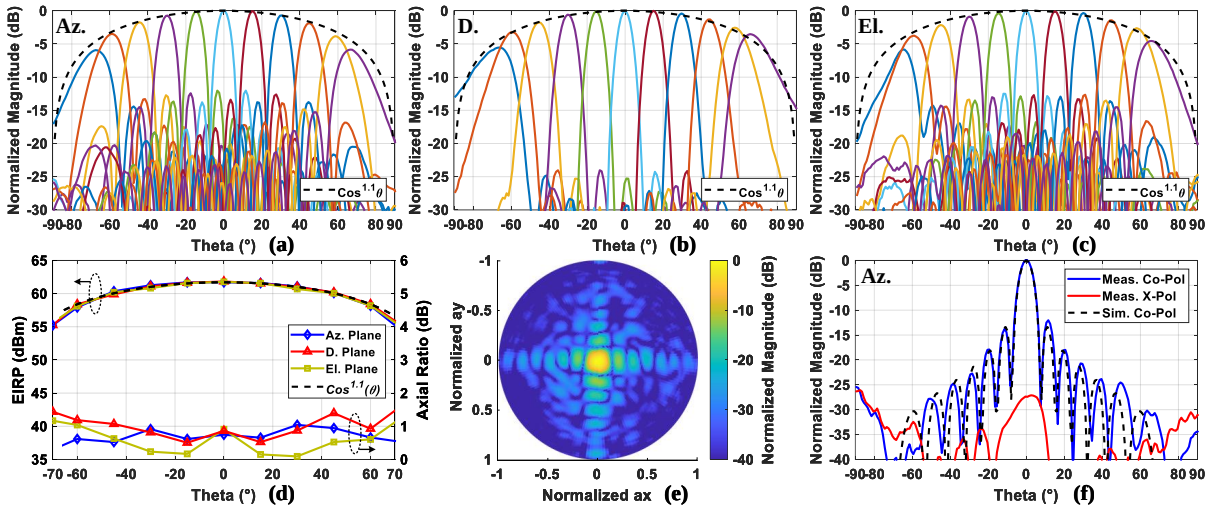

Figure 3.4: LHCP beams measured at 29 GHz uniform illumination: (a) Azimuth-plane scan, (b) Diagonal-plane scan, (c) Elevation-plane scan, (d) EIRP and axial ratio over various scans, (e) On axis 2-D pattern and (f) Azimuth cut-plane 1-D pattern.

The low calibration error is important when circular-polarization (CP) axial ratio (AR) is of concern, as seen in Fig. 3.4d. The phased-array achieved $<$ 1 dB AR on axis and $<$ 1.5 dB AR across all scans. This is equivalent to CP XPD of $>$ 25 dB on axis and $>$ 22 dB across all scans.

Fig. 3.4a to Fig. 3.4c present measured CP patterns as it scans in azimuth (Az), diagonal (D) and elevation (El) planes at 29 GHz. The phased-array scans to ± 60° with 3.3 dB loss and up to ±70° without grating lobes. These represent a near-ideal rolloff of $cos^{1.1}(\theta)$ in CP. The rolloff in H-plane and E-plane patterns when operating in single polarization is $cos^{1}(\theta)$ and $cos^{1.1}(\theta)$, respectively (not shown).

Fig. 3.4d presents the measured CP EIRP at 29 GHz versus scan. The phased-array achieves an EIRP of 60.5 dBm at P1dB and 62 dBm at saturation. This agrees well with the

calculated CP EIRP given by:

$$\begin{aligned} EIRP_{-1dB,CP} &= 20log_{10}(N) + G_{ant} + P_{element,CP} \\ &= 48 + 3 + 10 = 61\,dBm \end{aligned} \tag{3.1}$$

where

$$\begin{aligned} G_{ant} &= D_{ant} - loss \\ &= 10log_{10}(\frac{4\pi A_{element}}{\lambda^2}) = 3\,dB \end{aligned} \tag{3.2}$$

and D_{ant} is the directivity of an antenna element in a 4.67 mm x 4.67 mm grid, and loss is the total antenna and transmission-line loss between the chip and the antenna at 29 GHz. A P1dB of 10 dBm was taken since both V and H polarizations are summed for a circular-polarization measurement.

A 2-D pattern (Fig. 3.4e) and an Az. cut pattern (Fig. 3.4f) of the phased-array shows < -13 dB and < -24 dB sidelobe levels (SLL) in Az./El. and D. planes with > 25 dB XPD on axis. The 3-dB beamwidth of 6.8° in both Az. and El. planes agrees well with simulation. One can reduce SLL to < -20 dB on the principal planes using a 6-10 dB cosine amplitude taper.

3.4 Conclusion

This paper presents a planar, scalable, switchable dual-polarized 256-element Ka-band SATCOM TX phased-array with 32 dBW EIRP and which can scan to ±70° in all planes. Silicon beamformers and an all-planar construction ensure that such arrays are affordable and can be scaled to larger systems.

3.5 Acknowledgment

The authors thank Integrated Device Technology, IDT, for sponsoring the beamformer chips used in this work. The array was assembled by Kyocera International, San Diego, using their advanced phased-array assembly line. Measurements were performed in the ETS-Lindgren's AMS-5700 compact 5G antenna measurement system. This work was supported by IDT and Qualcomm.

Chapter 3, in part, is a reprint of the material as it appears in: K. K. Wei Low, S. Zihir, T. Kanar and G. M. Rebeiz, "A Scalable Switchable Dual-Polarized 256-Element Ka-Band SATCOM Transmit Phased-Array with Embedded RF Driver and ±70° Beam Scanning," *2020 IEEE/MTT-S International Microwave Symposium (IMS)*, Los Angeles, CA, USA, 2020, pp. 821-824, doi: 10.1109/IMS30576.2020.9223891. The dissertation author was the primary investigator and author of this paper.

Chapter 4

A 27-31 GHz 1024-Element Ka-Band SATCOM Phased-Array Transmitter with 49.5-dBW Peak EIRP, 1-dB AR, and $\pm 70^{\circ}$ Beam Scanning

4.1 Introduction

There is renewed interest in global space-based broadband connectivity envisioned by commercial enterprises with SATCOM systems such as Starlink, OneWeb, and Kuiper [16]–[17], and the new generation of systems promise high-speed, low-latency global coverage using low earth orbit (LEO) and medium-earth orbit (MEO) satellites. The move to lower orbit satellites was also enabled by recent advances of commercial silicon beamforming chipsets and affordable phased-arrays. With these chipsets, it is now feasible for user terminals to be outfitted with advanced active electronically-scanned phased-arrays (AESA) at relatively low cost (Fig. 4.1). Instead of traditional complex mechanical scanning units, the AESAs provide fast electronic

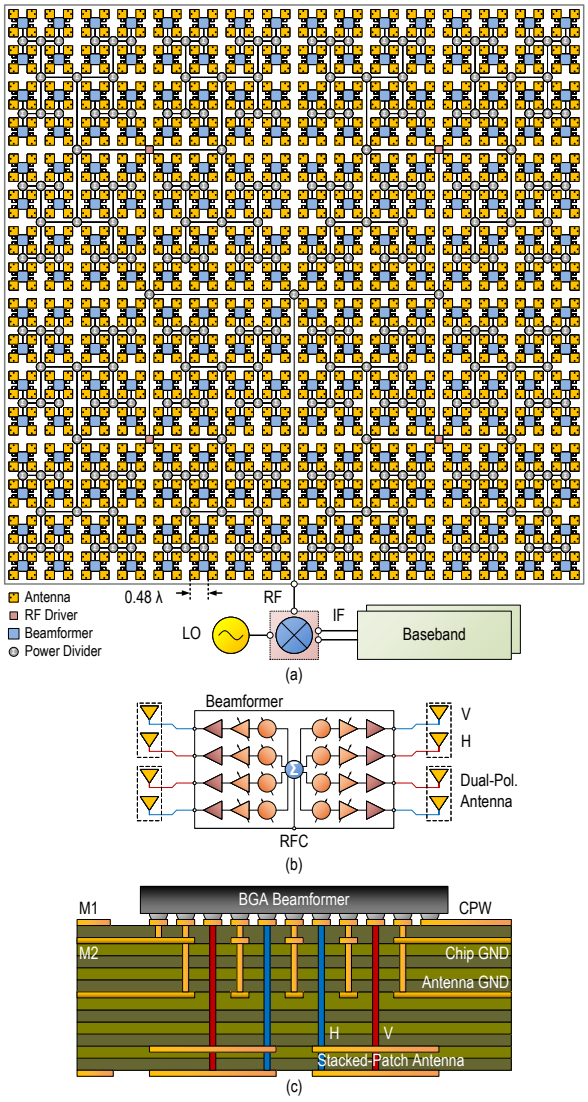

Figure 4.1: (a) Block diagram of the 1024-element phased-array. (b) 2 x 2 antenna cell with 8 channel TX beamformer. (c) PCB stackup.

beam-steering which is important for uninterrupted links between user terminals and moving satellites in LEO/MEO. Affordable phased-arrays also benefit current geostationary orbit (GEO) SATCOM systems especially for SATCOM-on-the-move systems [10]–[11].

In this paper, an expansion of [18], a wideband reconfigurable dual-polarized (DP) 1024-element Ka-band SATCOM TX phased-array is demonstrated with high peak EIRP, low cross-polarization and ability to scan in both planes (Fig. 4.1). Previously, various phased-arrays

at Ka-band were demonstrated with smaller apertures and some with a scan volume of less than 60° [13]–[15]. This work expands on [13]–[15] and demonstrates the use of quadrant RF drivers to ease the calibration and lower the input power requirement of large phased-arrays.

In Section II, we discuss the design of the phased-array from simulation to implementation. Measurements, both continuous wave and complex modulation, are presented in Section III and IV. The paper ends with a comparison with the state of the art and a conclusion.

4.2 SATCOM Phased-Array Transmitter Design

4.2.1 Architecture and Printed Circuit Board

Fig. 4.1(a) presents the architecture of the 1024-element Ka-band SATCOM phased-array transmitter with embedded drivers. It is based on a full RF beamforming architecture with 1024 dual-polarized antenna elements fed by 256 8-channel silicon beamformers. Each beamformer drives 4 dual-polarized antennas arranged on a 2x2 quad (Fig. 4.1(b)) and, together with RF/digital line drivers and other circuitry, are laid on a single printed circuit board (PCB).

The phased-array was designed to be scalable by cutting the PCB to the antenna grid on 3 sides. Doing so allows larger 2xN arrays, when tilted together, to synthesize patterns without grating lobes. A larger 4096-element phased-array for example, could be made with four 1024-element PCB and an additional external 1:4 power divider similar to [19]–[20] and without grating lobes.

Amplitude and phase on each dual-polarized antenna element can be independently controlled to transmit linear, rotated-linear, left- or right-hand circular polarization (CP).

Four 256-element subarray quadrants make up the 1024-element phased-array, each with separate RF driver (to overcome ohmic loss) and digital/power domains for redundancy. It can be programmed via high-speed 4-wire serial-peripheral interface (SPI) using an external microcontroller. The SPI lines were buffered using on-board digital line drivers to ensure signal

Table 4.1: Grating lobe scan limit and Scan blindness angle Summary

Square Grid d	0.48λ	0.49λ	0.5λ	0.51λ	0.52λ
Grating lobe scan limit (°)	-	-	90	73.9	67.4
Scan blindness angle (°)	-	76.3	68.5	63.1	58.6

- denotes out of visible region Note : Scan blindness result valid for λ/12 Megtron6 substrate

integrity when communicating with the board at high-speed.

Panasonic Megtron6 with ε_r = 3.26 and tanδ = 0.005 at 30 GHz was used for the PCB stackup (Fig. 4.1(c)). Layer M1 was used primarily for the RF beamforming network (BFN) with M2 for ground. Other layers were used for digital control, power and the antenna ground. Components compatible with surface mount technology (SMT) were used in the design and they were soldered on the top layer (M1) with antennas on the underside. The PCB is about 1.5 mm thick.

4.2.2 Infinite Array Antenna Unit Cell

Fig. 4.2(a) presents the unit cell 3D model of the planar dual-linear polarized stacked-patch microstrip antenna. The antenna was simulated in an infinite array electromagnetic (EM) simulator. The stacked-patch microstrip antenna was chosen for ease of integration and manufacturing, dual-polarization capability, and has relatively wide bandwidth (BW).

It is well known that microstrip antenna with a single patch is narrowband with about 5% impedance bandwidth while probe-fed stacked-patch microstrip antenna with double-tuned resonance has been shown to cover a wide bandwidth of 10%-20% [21]. This make it suitable to cover the SATCOM Ka-band 27 to 31 GHz uplink frequency range (14%).

There are various ways to generate circular polarization using microstrip patch antennas. These include modification to the shape of the patch (technique 1) [22]–[23], applying sequential phase rotation to neighboring patches (technique 2) [21,24], and combining dual linear-polarization

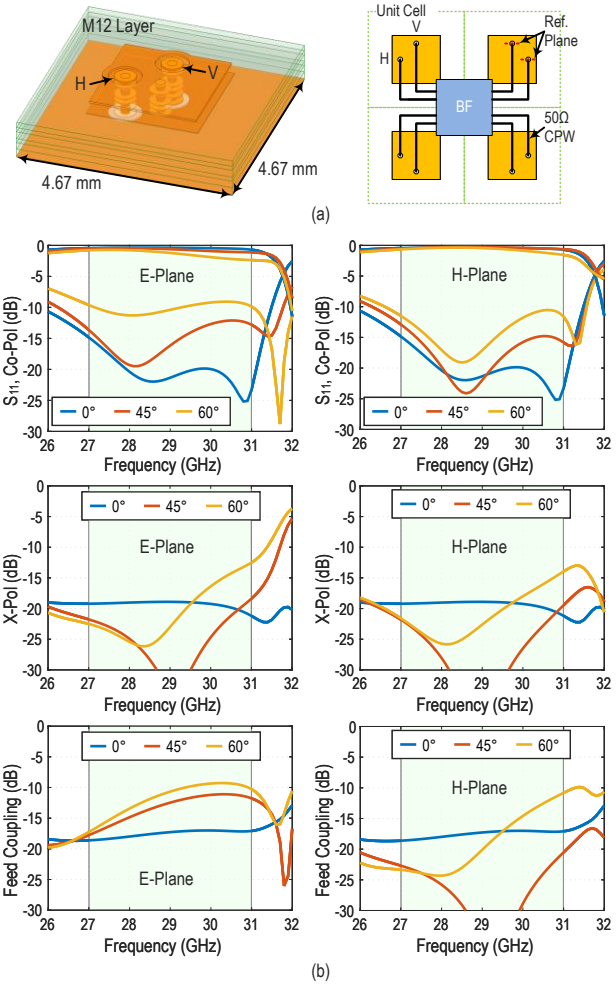

Figure 4.2: (a) Unit cell 3D model of the dual-polarized stacked-patch microstrip antenna and its placement in the sequentially rotated 2 x 2 antenna cell. (b) HFSS simulation of the unit cell under different scanning condition.

with the appropriate phasing (technique 3) [19]–[22]. Technique 1 is simple but produces a narrow circular axial ratio (AR) 3dB bandwidth. Technique 2 produces wide AR bandwidth (nested variants up to 32% reported in [25]) but AR can suffer at high scan angles. Technique 3, used in this work, also produces wide AR bandwidth but the AR does not suffer at higher scan angles since the amplitude and phase of each channel can be continuously adjusted versus scan angle. Its implementation is straight forward with the 8-channel beamformer, with independent controllable amplitude and phase, and allows the generation of all possible polarizations (linear, rotated linear, left- and right-hand circular polarization).

The antenna elements were placed in a square grid of 4.67 mm which is 0.48λ at the highest operating frequency of 31 GHz. A square/rectangular grid is simpler to implement than triangular grid even though triangular grid maximizes scan volume. A 0.48λ grid is chosen for the array and ensures no vestige of the grating lobe falls in the visible region when scanning. The grid distance to ensure this condition can be calculated from the array factor [26]-[27] using:

$$d < \left(\frac{N_d - 1}{N_d}\right)\frac{\lambda}{2} \tag{4.1}$$

where N_d is the number of elements in a linear array. The grid allows the phased-array to scan to ±75° and results in a directivity of 4 dB per element at 29 GHz (mid-band)

$$D_{element} = 10log_{10}\left(\frac{4\pi D_x D_y}{\lambda^2}\right) = 4\,dB\,|_{29\,GHz} \tag{4.2}$$

where D_x, D_x are dimensions of the grid. The directivity of the 1024-element phased array is 34.1 dB with a 3-dB beamwidth of 3.7° under uniform illumination

$$D_{array} = D_{element} + 10log_{10}\,(1024) = 34.1\,dB\,|_{29\,GHz} \tag{4.3}$$

Another consideration for grid sizing is scan blindness. It occurs when the propagation constant β equals a surface wave propagation constant β_{SW} [28]. This is usually the dominant TM0 surface wave mode (for grounded dielectric slab) and scan blindness leads to severe mismatch in input impedance or, equivalently, a significant dip in the active element pattern near scan angles where the array is 'blind'. Numerical calculation of the blindness angle shows that blindness angle θ, for square 0.48λ grid, does not fall on the real axis (imaginary). This indicates that scan blindness will never occur in the visible region for this design. Table 4.1 summarizes the grating lobe scan limit and scan blindness angle versus various square grid spacing d.

Fig. 4.2(b) presents the EM simulated performance of the antenna, as the array scans to 60°, with the reference plane on M1. The antennas are well matched with S_{11} less than -15 dB

Table 4.2: TX SiGe Beamformer Summary

Parameter	Unit	F6502
Frequency	GHz	27-31
No. of Channels	-	8
Typical Gain	dB	25
Phase Shifter	bit	6
Phase Step	°	5.625
VGA	bit	6
VGA Step	dB	0.5
OP_{1dB}	dBm	10[1]
Power/channel	mW	150[1]
Supply Voltage	V	2.1-2.5

[1] At 2.3V, nominal bias setting, P_{1dB}

and remains less than -9 dB for both H- and E-plane as the array scans. This translates to high transmission of co-polarization (includes ohmic, dielectric, and mismatch losses) of more than -1 dB on axis and remains better than -2 dB to ±60° in both planes.

One factor for higher E-plane input mismatch is due to energy coupling from antenna to surface wave as the array scans. This also decreases the cross-polar discrimination (XPD) and increases feed coupling between the two polarization, input of one feed to the input of the other, in the E-plane. Despite this, the feed coupling starts below -17 dB and remains less than -9 dB across scan, while the cross-polarization (X-pol) component is less than -19 dB and remains below -13 dB across scan for both polarizations.

A technique of sequentially rotating the antenna feeds in a 2 x 2 antenna cell, well covered in previous publications [18]–[29], further improves XPD by providing rotational symmetry. When implemented in a 2 x 2 antenna cell, the symmetry provides X-pol cancellation in both principal planes and various nulls off axis without the need for a balanced structure [30]–[31]. D-plane performance is approximately the average of H-plane and E-plane (not shown for brevity).

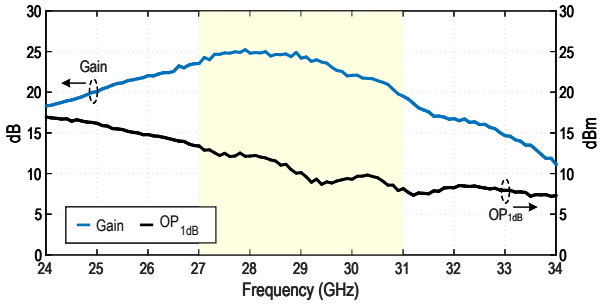

Figure 4.3: Measured Gain and OP_{1dB} of the F6502 beamformer chip.

4.2.3 Ka-Band Transmit Beamformer Chip

The Renesas F6502 is a first-generation silicon 8-channel transmit (TX) beamformer (BF) chip designed for Ka-Band SATCOM frequency division duplexing (FDD) phased-array applications (Fig. 4.1(b)). Table 4.2 summarizes the key chip performance parameters and Fig. 4.3 presents the measured gain and OP_{1dB}.

The BF chip can be used to drive up to four dual-polarized antennas or eight single-polarized antennas. Each channel has independently controllable amplitude and phase via SPI. The F6502 is available in a ball grid array (BGA) package with 0.5 mm ball pitch, and is 3.8 mm x 4.6 mm.

4.2.4 Beamforming Network and RF Driver

The RF input to the array is distributed to the 256 beamformers using 1:256 corporate Wilkinson power divider network with embedded RF drivers and standard 0201 sized SMT resistors on M1 (Fig. 4.4(b)), and its equivalent circuit is shown in Fig. 4.4(a). The EM simulated insertion loss of the Wilkinson power divider was about 0.3 dB, with an input return loss more than 18 dB, output return loss more than 22 dB, and isolation more than 20 dB in the band of interest (Fig. 4.4(c)). The BFN uses an equi-length H-topology and this leads to equal group delay from array input to every antenna. Equi-length topology simplifies calibration and reduces beam squint.

Fig. 4.5 presents the RF system analysis. Four beamformers were used in each 256-element

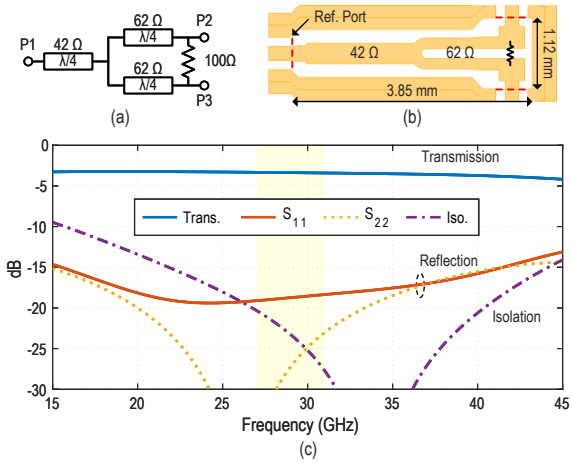

Figure 4.4: (a) Equivalent circuit of the CPW wilkinson power divider, (b) layout on M1, (c) and EM simulation response.

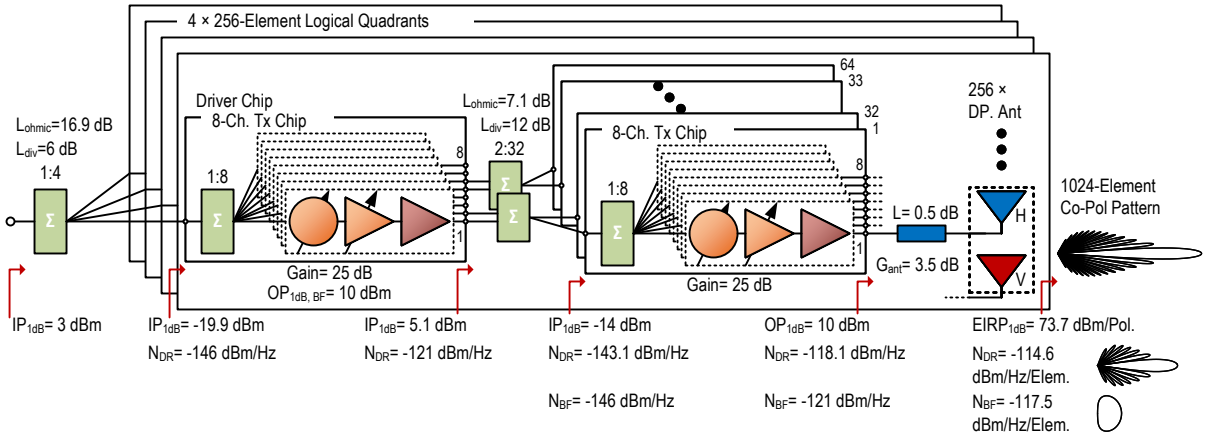

Figure 4.5: RF system analysis block diagram of the 1024-element phased-array showing compression point (P_{1dB}), effective isotropic radiated power (EIRP), and radiated in-band TX noise (N_{DR}: Noise due to driver chip, N_{BF}: Noise due to beamformer).

quadrant as RF drivers to overcome ohmic loss, division loss, and reduce input P_{1dB} driving requirement. SATCOM transmitters often drive their systems to P_{1dB} to improve their efficiency, and without embedded drivers, a 1024-element array will require

$$
\begin{aligned}
IP_{1dB,no\,driver} &= IP_{1dB,BF} + L_{ohmic} + L_{div,1:256} \\
&= -14\,dBm + 24\,dB + 21\,dB \\
&= 31\,dBm
\end{aligned}
\tag{4.4}
$$

at the common RF port (input port), which is high. Hence, beamformers were used as RF driver in the center of each quadrant reducing the IP_{1dB} to 3 dBm at the RF input. The RF signal into the driver is split and amplified from four output channels with each 128-element halves of the 256-element logical quadrant driven from two channels to improve redundancy.

Using beamformers as RF driver has also the benefit of providing the ability to control mean phase and amplitude of each quadrant. This allows for calibration at the subarray level, to correct for mean-to-mean variation between subarrays, and preserves the gain dynamic range of individual channels feeding each element. This is especially useful to correct for the different loss and phase mismatch of different cables when building even larger phased-arrays. Also, about 5 dB of additional $OP1dB$ capabilities was budgeted in the RF chain, and enables the RF driver chip to drive the phased-array to P_{1dB} with complex modulated waveform peak-to-average power ratio (PAPR) without degrading the waveform error vector magnitude (EVM).

One issue to consider with embedded RF drivers, however, is the radiated in-band output noise. Unlike the incoherent output noise from individual beamformer or from transmit/receive (T/R) modules, the noise from the embedded drivers is coherent and therefore radiate with an array factor (AF) depending on the driven subarray. The measured output noise of the beamformer driver is -121 dBm/Hz per channel and is coherently distributed to 32 beamformers. This is then amplified and results in 128-elements transmitting a coherent noise (N_{DR}) of -118.1 dBm/Hz/element. This is comparable to the incoherent output noise (N_{BF}) of -121 dBm/Hz/element. The coherent noise will radiate with the AF of 128-elements and scans with the main beam while the incoherent noise radiated follows the element pattern of the antenna

and does not scan. Knowing that waveform bandwidth is up to 400 MHz, the equivalent coherent output noise can be up to -32 dBm/channel and is much lower than the radiated power of 10 dBm/channel, and with a radiated SNR of 42 dB (SNR of 52 dB for a 40 MHz bandwidth waveform). This shows that, when designed correctly, the driver output noise is not a significant contributor to the array EVM (0.3-1% EVM degradation).

4.3 Calibration and Measurements

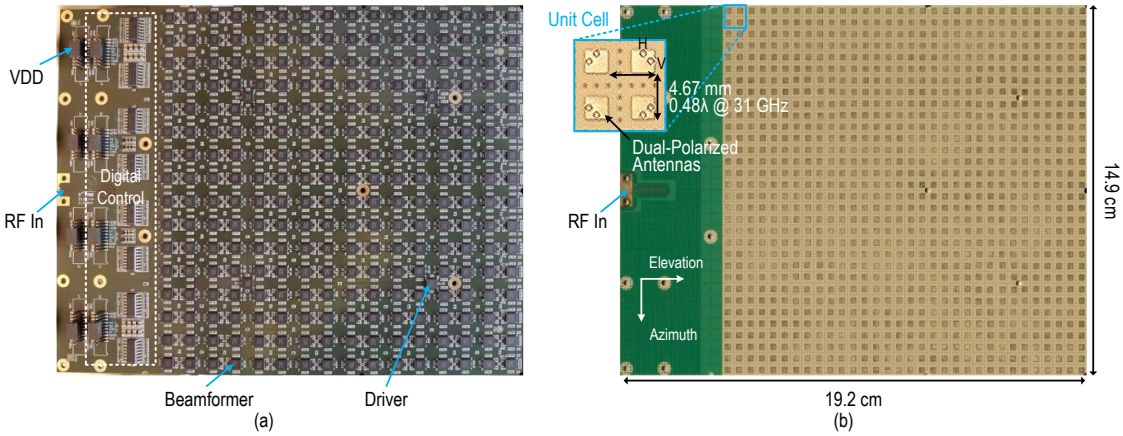

Figure 4.6: (a) Component side view and (b) antenna side view of the 1024-element phased-array showing sequential rotation in the 2 x 2 antenna cell.

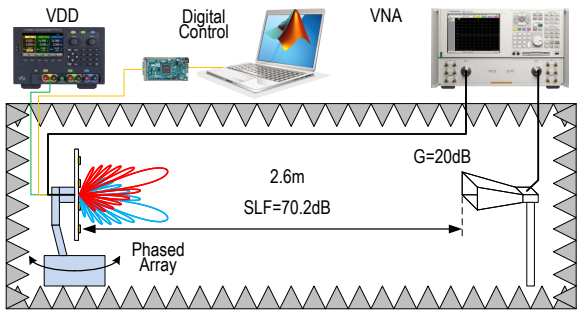

Figure 4.7: Calibration and far-field measurement setup.

Fig. 4.6 presents the fabricated PCB with 256 F6502 chips, 4 driver chips, SPI drivers, and SPI and power connectors. The 1024-element phased-array was measured in an anechoic

chamber with measurement range $R_{chamber}$ = 2.6 m which places the array at the far-field between $\frac{D^2}{\lambda}$ and $\frac{2D^2}{\lambda}$ (Fig. 4.7). The far-field range (R_{FF}) of the 1024-element phased-array is

$$R_{FF,1024} = \frac{2L^2}{\lambda} = 4.3\,m\,|_{29\,GHz} \tag{4.5}$$

where L is the dimension of the array.

Pattern measurements were done on a single axis rotary platform using a Keysight vector network analyzer (VNA) and standard gain horn (G_{horn} = 20 dB). The array is powered by a Keysight power supply and fans were used to cool the phased-array, keeping it under 55 °C.

The phased-array could be operated without calibration but with reduced performance like increased sidelobe, wider beamwidth, and lower EIRP even though care was taken to design the array to be as symmetrical as possible. A single calibration profile is all that is needed for most operation, as long as the operating frequency does not differ from calibration frequency significantly. For this work, only a single calibration was done at 29 GHz.

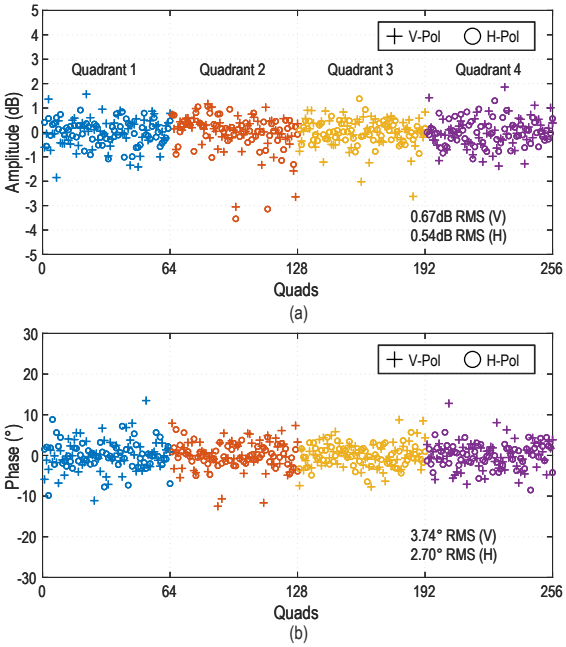

Figure 4.8: (a) Residual amplitude and (b) phase errors after calibration.

Calibration was done on axis at mid-band (29 GHz), by measuring the individual antenna

response and correcting for the phase and amplitude errors between them. There are two major steps in the calibration procedure. First, subarray-level calibration is done by removing the mean amplitude and phase variance between the 256-element logical quadrants using the RF drivers on each quadrant. As described earlier, using RF drivers for the first calibration step preserves gain dynamic range of individual channels. Next, a series of calibration iteration were executed, on a quad or element level, until desired root-mean-square (RMS) phase and RMS amplitude targets were met using beamformers. The calibration procedure resulted in 0.67 and 0.54 dB RMS residual amplitude error, and 3.74 and 2.7° RMS residual phase error, for V-polarized and H-polarized quads, respectively (Fig. 4.8). There may be some outliers due to component, fabrication, or assembly issues but, to a large extent, they do not affect the operation of large phased-arrays.

After calibration, the phased-array beam can be scanned by applying phase shifts on each element along the scan direction with

$$\alpha_x = kD_x sin(\theta_0) cos(\phi_0) \tag{4.6}$$

$$\alpha_y = kD_y sin(\theta_0) sin(\phi_0) \tag{4.7}$$

where α_x, α_y are incremental phase shift to be applied on the x- and y-th elements and θ_0, ϕ_0 is the direction in which the phased-array beam should be directed/scanned to.

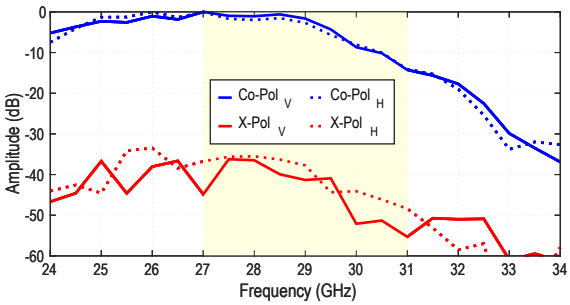

Figure 4.9: Measured co- and cross-pol frequency response on axis.

Fig. 4.9 presents the measured broadside co- and cross-pol of both vertical and horizontal (linear) polarization frequency response of the 1024-element phased-array. The co-pol frequency response follows closely to the beamformer measured response. Cross-pol. levels of about 35 dB are achieved due to the feed rotation described in section II. Also, any rotated linear polarization could be generated by varying the amplitude of the V- and H-polarization, either in-phase or out-of-phase, so as to achieve a polarization angle of

$$\varphi = atan2(|V|, |H|) \tag{4.8}$$

where $atan2$ is the 2-argument arc-tangent (tan^{-1}) function.

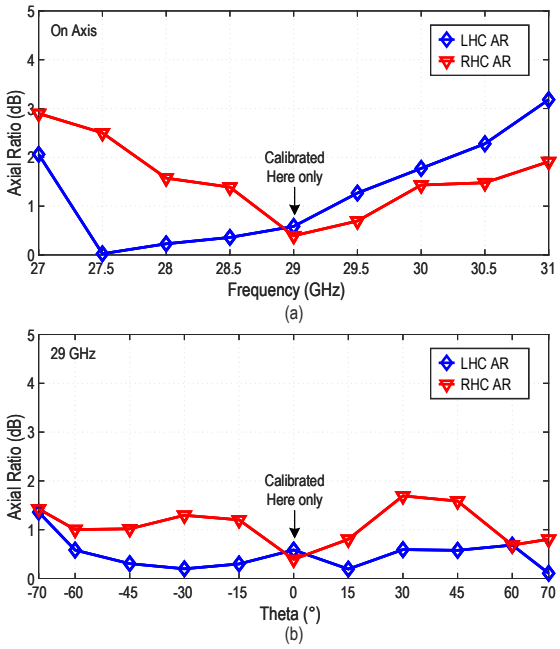

Figure 4.10: (a) Measured AR versus frequency and (b) scan after calibration.

Left- and right-hand circular polarization (CP) are generated with the appropriate 90° shift between the V- and H- polarizations, and their measured axial ratio (AR) are shown in Fig. 4.10. It can be seen that less than 1 dB AR was achieved on axis at 29 GHz and under 1.8 dB from 28 to 30 GHz for both left- and right-hand CP. As the array scans to ±70°, the AR degrades only by about 1.5 dB across scan at 29 GHz. This is an equivalent CP XPD of more than 25 dB

on axis and more than 19 dB across scan with only one calibration.

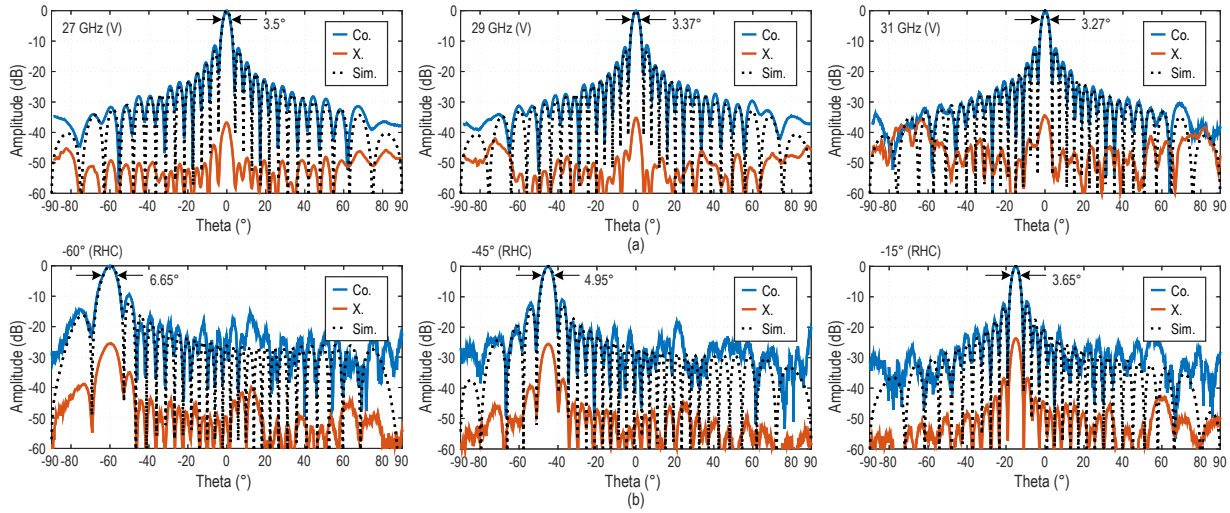

Figure 4.11: (a) Measured co- and cross-polarization for vertical polarization at 27, 29, and 31 GHz (H-plane). (b) Measured 29 GHz right-hand circular co- and cross-polarization when scanned to -60°, -45°, and -15° off axis. The 1024-element phased-array was calibrated only once on axis at 29 GHz.

4.3.1 Patterns

Fig. 4.11(a) shows measured co- and cross-polarization V-pol patterns at 27, 29, and 31 GHz with less than -12 dB sidelobe level (SLL) and less than 3.5° half-power beamwidth (HPBW) on axis under uniform illumination. The co-pol follows closely to the ideal simulated pattern and cross-pol remains lower than -35 dB and it remains less than -26 dB across scan (not shown). Fig. 4.11(b) shows measured co- and cross-polarization right-hand circular (RHC) polarization patterns scanned to -60°, -45°, and -15° at 29 GHz are shown with CP XPD more than 23 dB as it scans. Better CP XPD (more than 27 dB) were achieved with left-hand circular (LHC) polarization across scan (not shown) for this calibration profile.

Fig. 4.12 presents superimposed beam patterns as the phased-array scans to ±70° at 29 GHz and without grating lobes. The scans in H-plane (Fig. 4.12(a)) and E-plane (Fig. 4.12(c)) rolloff to $cos^{1}(\theta)$ and $cos^{1.1}(\theta)$, respectively, while combined dual-polarized patterns such as LHC-pol (Fig. 4.12(b)) rolloff to $cos^{1.1}(\theta)$. This means that the scan loss at 60° is only -3 to -3.3

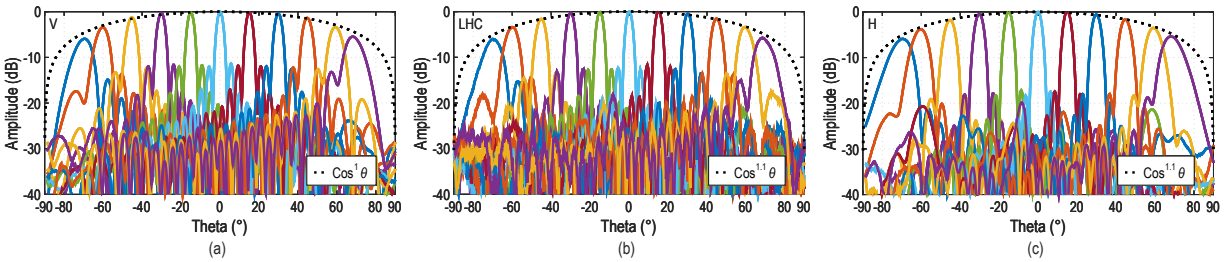

Figure 4.12: Measured 1024-element phased-array scanned beams at 29 GHz to ±70°. (a) Vertical polarization (H-plane). (b) Left-hand circular polarization. (c) Horizontal polarization (E-plane) under 6-dB raised cosine taper. Scan drop for right-hand circular polarization tracks $cos^{1.1}(\theta)$ (not shown).

dB.

The patterns maintains less than -12 dB SLL under uniform illumination (Fig. 4.11 to Fig. 4.12(b)) and can be improved to less than -18 dB SLL with a 6-dB raised cosine taper (Fig. 4.12(c)). Lower SLL can be achieved using a more aggressive amplitude taper. Patterns along D-plane were similar but with better SLL (less than -24 dB under uniform illumination) as expected of rectangular aperture. The measurements also prove the validity of our calibration method.

4.3.2 Beam-Squint

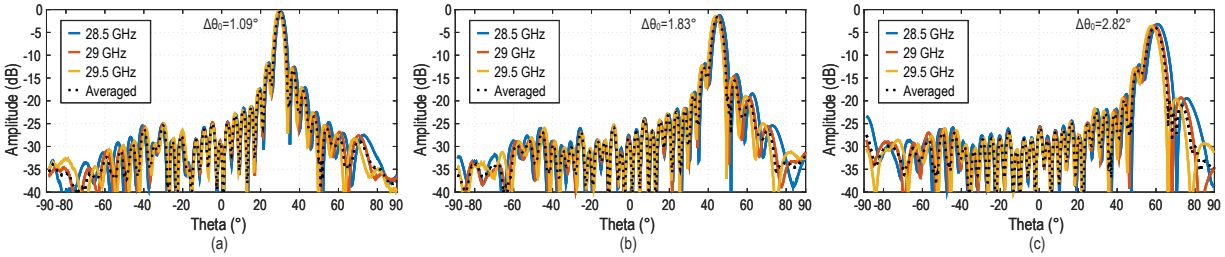

Figure 4.13: Measured 1024-element phased-array beam-squint ($\Delta\theta_0$) from 28.5 to 29.5 GHz when scanned. (a) 30°. (b) 45°. (c) 60°. There are no/negligible squinting near axis and amplitudes are normalized to the axis at 29 GHz (not shown). Real-world SATCOM application uses lower bandwidths.

Fig. 4.13 shows the measured beam-squint ($\Delta\theta_0$) of the 1024-elements phased-array for a 1 GHz bandwidth with center frequency at 29 GHz. Beam-squint is the measure of pointing error between different frequencies of the phased-array :

$$\Delta\theta_0 = (\theta_0 + \Delta\theta) - \theta_0 \tag{4.9}$$

where θ_0 is the beam at f_0 and $(\theta_0 + \Delta\theta)$ is the beam at $(f_0 + \Delta f)$. The relationship between $\Delta\theta_0$ and Δf can be estimated in [32].

The measured beam-squint when the phased-array is scanned to 30°, 45°, and 60° is low at 1.09°, 1.83°, and 2.82° respectively. There is no beam-squint when the phased-array beam is on axis ($\Delta\theta_0 = 0$) due to the use of equi-length BFN.

Beam-squint increases with increasing signal fractional bandwidth (FBW) and beam scan angle (θ_0). With the narrower channel bandwidth of SATCOM Ka-band (400 MHz), beam-squint will be less than 1.4° when scanned to 60° which is low. Beam-squint can be eliminated using true time delay (TTD) instead of phase shifter (PS), with constant phase characteristic, on every element or at least mitigated by using TTD on a subarray level. Narrower signal bandwidth will in turn make beam-squint negligible [33].

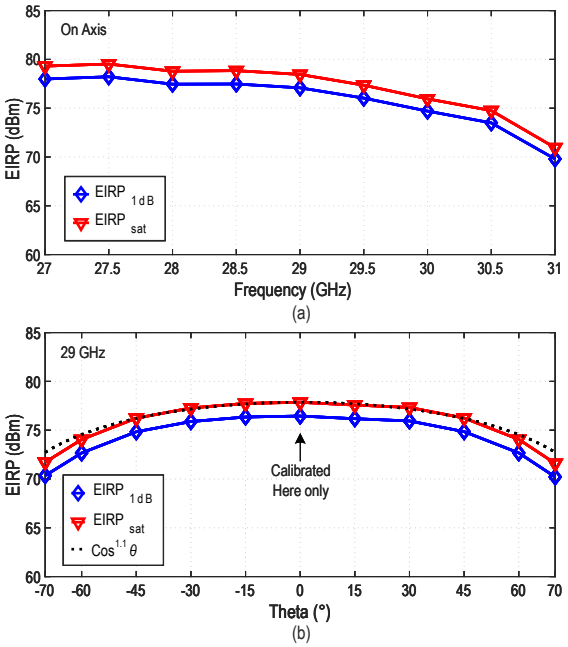

Figure 4.14: (a) Measured CP EIRP versus frequency and (b) scan angle.

There is also the question of inter-symbol interference (ISI) in large phased-arrays, but it

can seen in [34] that ISI can be compensated using equalization during post processing in the digital domain.

4.3.3 EIRP

The 1024-element phased-array EIRP in CP was measured across frequency on axis (Fig. 4.14(a)) and across scan at 29 GHz (Fig. 4.14(b)). The phased-array achieves an EIRP of 76 dBm (46 dBW) at P_{1dB} and 78 dBm at saturation (48 dBW) in CP at 29 GHz. This is 73 dBm EIRP per polarization at P_{1dB} and agrees well with the calculated $EIRP_{1dB}$ given by:

$$\begin{aligned} EIRP_{1dB}/Pol. &= 20log_{10}(1024) + G_{ant} + P_{elem.} \\ &= 60.2 + 3.5 + 10 \\ &= 73.7\,dBm/Pol.|_{29\,GHz} \end{aligned} \tag{4.10}$$

and with + 3 dB for circular polarization.

$$\begin{aligned} G_{ant} &= D_{ant} - L_{ohmic} \\ &= 3.5\,dB\,|_{29\,GHz} \end{aligned} \tag{4.11}$$

where L_{ohmic} is the total loss from the antenna to the beamformer. $P_{elem.}$ is the output power of the BF chip and, at P_{1dB}, this is 10 dBm/channel at 29 GHz and 12.5-13 dBm/channel at 27-28 GHz (Fig. 4.3). The higher P_{1dB} made it possible for the phased-array to achieve a peak EIRP of 79.5 dBm (49.5 dBW) at 27-27.5 GHz (Fig. 4.14(a)).

The measured CP EIRP roll-off versus scan closely match the antenna's $cos^{1.1}(\theta)$ element factor at 29 GHz. Measured roll-off for other frequencies are similar (not shown). At P_{1dB}, the 1024-element phased-array consumes 169.2 W for 46 dBW EIRP at 29 GHz in CP mode, 280.5

W for 49.5 dBW at 27.5 GHz, and does not take into account four 3.5 W fans cooling the array.

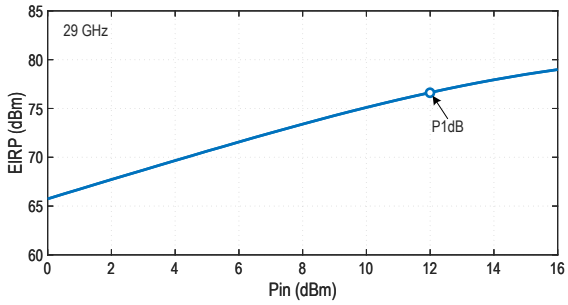

Figure 4.15: Measured CP EIRP versus Pin (referenced to the connector).

The EIRP versus Pin at 29 GHz is presented in Fig. 4.15 and 12 dBm is required at the connector to drive the phased-array to P_{1dB}. The higher IP_{1dB} is due to decreased electronic gain during phased-array calibration and reinforces the importance of the embedded RF drivers for large phased-arrays.

An $EIRP_{1dB}$ of 58 dBW and a 3-dB beamwidth of 1.7° on axis at 29 GHz can be achieved with four of these arrays assembled together in a 4096-element phased array, suitable for GEO systems. This would result in an $EIRP_{1dB}$ of 54.7 dBW and 3-dB beamwidth of 3.4° at 60° scan angles (52.5 dBW, 5° beamwidth at 70° scan).

4.4 Complex Waveform Measurements

The Keysight VXG vector signal generator and Keysight UXA signal analyzer were used measure the phased-array performance when transmitting digital modulated waveforms. Phase shift keying (PSK) is commonly used in SATCOM applications as it has constant power envelope (maximize power efficiency) without sacrificing bandwidth efficiency.

In the following measurements, QPSK (2 bits/symbol), 8-PSK (3 bits/symbol), and 16-QAM (4 bits/symbol) waveforms are presented. Note that, for modulation with 4 bits/symbol, 16-APSK is generally used instead of 16-QAM for SATCOM applications. 16-APSK modulation

is more robust against fluctuation in amplitude compared to 16-QAM, which is great for operation at P_{1dB}, but it is generally easier to compare transmitter performance using 16-QAM instead.

The various measurements were measured with a root raised cosine filter (α) of 0.35. With $\alpha = 0.35$, the PAPR for QPSK and 8-PSK are 3.7 dB, and the PAPR for 16-QAM is 4.6 dB. In this work, the measured EVM_{RMS} is calculated as :

$$EVM_{RMS} = \frac{\sqrt{\frac{1}{M}\sum_{m=1}^{M} err[m]^2}}{RMS\ of\ Constellation} \times 100\% \tag{4.12}$$

4.4.1 ACPR

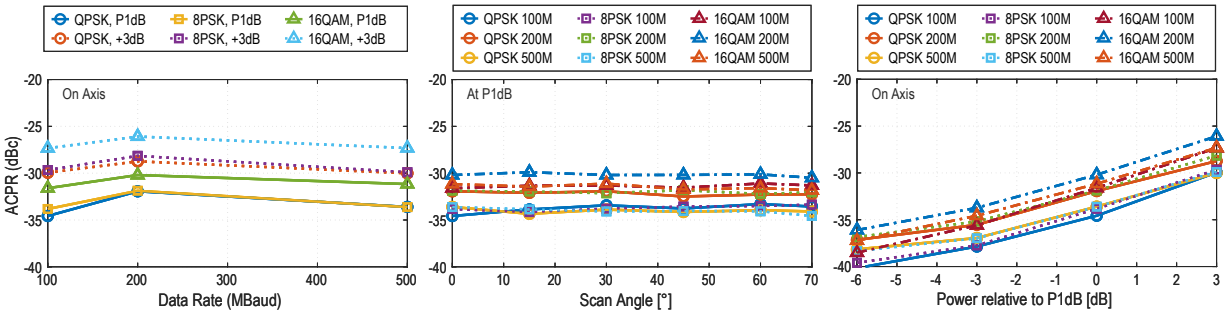

Figure 4.16: Measured adjacent channel power ratio (ACPR) for various data rate, scan, and P_{1dB} backoff for QPSK, 8-PSK, and 16-QAM modulation.

Fig. 4.16 presents the measured adjacent channel power ratio (ACPR) of QPSK, 8-PSK, 16-QAM modulation under different data rate at P_{1dB} and $P_{1dB} - 3dB$, scan angles to 70° at P_{1dB}, and various backoff from P_{1dB}.

At P_{1dB}, the ACPR remains below -33 dBc for QPSK, 8-PSK and below -31 dBc for 16-QAM modulation from 100 to 500 MHz baudrate on axis. The ACPR only degrades about 1 dB across scan at P_{1dB} for these modulation from 100 to 500 MHz. At lower power levels on axis, the ACPR improves, and is less than -35c dB at 100 to 500 MHz. These results are achieved without any linearization and show the phenomenal performance of phased-arrays at P_{1dB} operation.

4.4.2 EVM

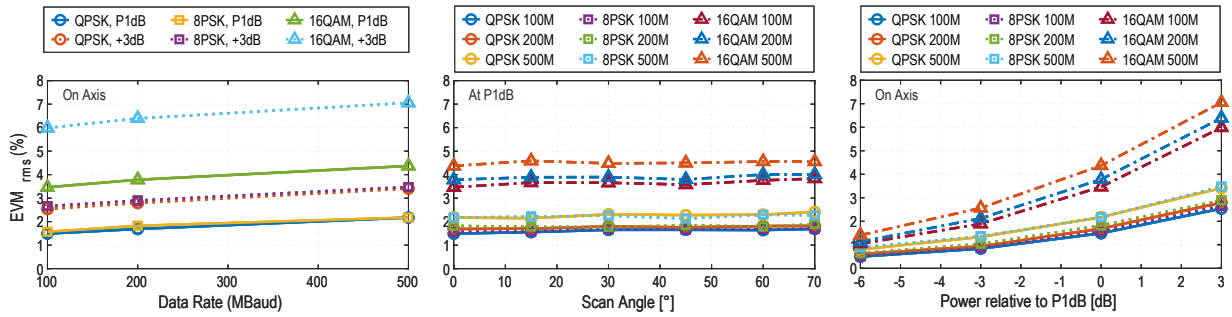

Figure 4.17: Measured error vector magnitude (EVM_{rms}) for various data rate, scan, and P_{1dB} backoff for QPSK, 8-PSK, and 16-QAM modulation.

Fig. 4.17 presents the measured EVM for the phased-array with EVM_{setup} de-embedded from measurement using :

$$EVM_{array} = \sqrt{EVM_{meas}^2 - EVM_{setup}^2} \ \ [\%] \tag{4.13}$$

and EVM_{setup} ranges from 0.5-1.5% depending on specific settings used. At P_{1dB}, the EVM remains below 2.1% for QPSK, 8-PSK and below 4.3% for 16-QAM modulation from 100 to 500 MHz baudrate on axis. The EVM degrades by only 0.2% across scan at P_{1dB} for QPSK and 8-PSK waveforms (less than 0.35% for 16-QAM). At lower power levels on axis, the EVM is about 1% for 100 to 500 MHz. Fig. 4.18 and Fig. 4.19 presents the measured phased-array constellations at P_{1dB} across scan and for various baudrates, and near ideal performance is achieved.

The low ACPR and EVM with QPSK and 8-PSK modulation means that the phased-array can be operated at P_{1dB} without backoff for higher efficiency. This is beneficial for SATCOM applications where high EIRP is needed.

Fig. 4.20 presents the measured EVM versus of active elements in a phased-array at P_{1dB}. EVMs of various active groups of N elements of the phased-array were measured from N = 4 to 1024. As number of active elements is reduced, the measurement range is decreased

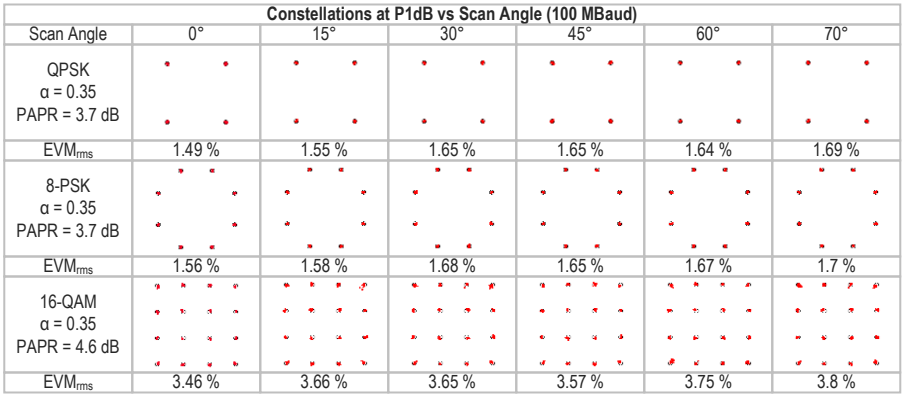

Figure 4.18: Measured EVM_{rms} constellations versus scan at P_{1dB} with 100 MBaud waveforms.

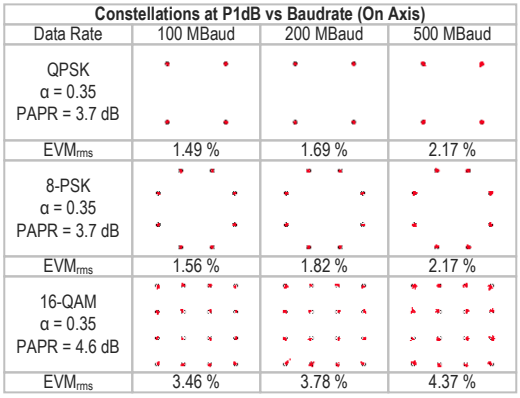

Figure 4.19: Measured EVM_{rms} constellations versus data rate at P_{1dB}.

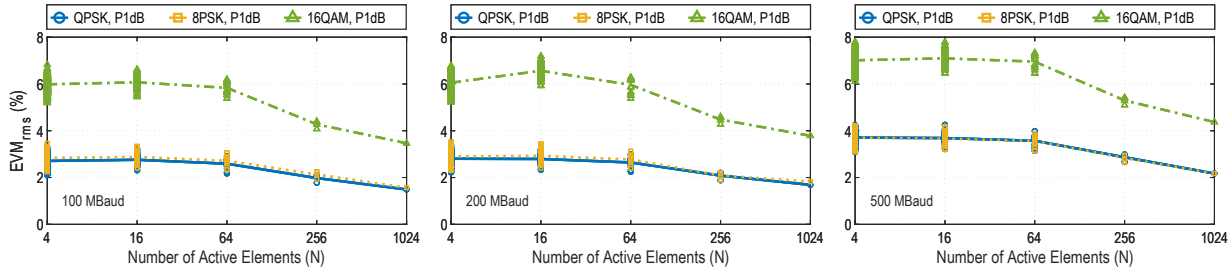

Figure 4.20: Measured EVM versus number of active elements for various data rate at P_{1dB} for QPSK, 8-PSK, and 16-QAM modulation. Measured distributions are shown in vertical bars and mean EVMs are shown with solid lines.

as well to ensure that the measurement is not noise-limited (still in the far-field). It is seen that the mean EVM improves as the size of phased-array increases. This has been shown before in different publications and large phased-arrays provide better EVM performance than smaller

Table 4.3: Comparison with State-of-the-art Ka-band SATCOM Phased-Array Transmitters

Parameter	This Work	UCSD [13]	UCSD [37]	UESTC [38]	C-COM [15]
Frequency (GHz)	27 - 31	28 - 31	27 - 31	29.5 - 30	27.5 - 31
Fractional BW (%)	13.8	10.2	13.8	1.68	12
No. of Elements	32x32 (Tx)	16x16 (Tx)	16x16 (Tx)	32x32 (Tx)	16x16 (Tx)
Lattice Topology	Rectangular	Rectangular	Rectangular	Rectangular	Rectangular
Lattice[1] (mm)	4.67 / 4.67	8.75 / 4.67	4.67 / 4.67	5 / 5	–
Polarization	DP-Linear	DP-Linear	DP-Linear	DP-Circular	SP-Circular
HPBW on Axis[1] (°)	3.37 / 3.37	3.5 / 7	6.8 / 6.8	3.2 / 3.2	6.5[+]
Scan Range[1] (°)	±70 / ±70	±60 / ±5	±70 / ±70	±60 / ±60	±70 / ±70
60° Scan Loss[1] (dB)	-3.3 / -3	-3.7 / –	-3.3 / -3	-4.5 / -4	-3[+]
Sidelobe[2] (dB)	<-12 / <-22[@]	<-13	<-13 / <-24[@]	<-10	<-10
XPD on Axis[3,4] (dB)	>35	>21	>25	–	–
XPD vs Scan[3,5] (dB)	>26	–	>22	–	–
AR on Axis[4] (dB)	<3 / <1[#]	<6 / <2[#]	<1[#]	<2	–
AR vs Scan[5] (dB)	<2	–	<1.5	<14 / <3[$]	–
$EIRP_{1dB}$[4,6,7] (dBW)	46 / 48	33.5	30.5	42.5 - 45	34.5
$EIRP_{sat}$[4,6,7] (dBW)	48 / 49.5	34.5	32	–	–
P_{DC}[6,8] (W)	169.2 / 280.5[*]	57.6	–	108	–
$P_{DC}/Ch.$[8,9] (mW)	82.6 / 136.9[*]	112.5	–	105.5	168.75
Size (cm^2)	14.9 x 19.2	7.48 x 14	7.47 x 11.68	16 x 21	–

[1] Elevation/Azimuth or E-Plane/H-Plane [2] Uniform Illumination [3] Linear-Polarization
[4] Operating Frequency [5] Operating Scan Range [6] Circular-Polarization or Dual-Polarization Mode
[7] On Axis (Broadside) [8] At P_{1dB} [9] Calculated from P_{DC}/No. of Elements [+] From Graph
[@] D-Plane [#] Near Calibration Frequency or Mid-band [$] Up to ±30° Scan
[*] 46 dBW/169.2W/82.6mW at 29 GHz $P1dB$ 48 dBW/280.5W/136.9mW at 27.5 GHz $P1dB$

arrays. Explanations and additional measurements are shown in [35]–[36].

Table 5.2 summarizes the performance of the 1024-element dual-polarized phased-array and compares it with other state-of-the-art SATCOM Ka-band phased-array transmitter.

4.5 Conclusion

A wideband 27-31 GHz dual-polarized Ka-band 1024-element phased-array transmitter for SATCOM was presented with a peak EIRP of 49.5 dBW at 27.5 GHz (48 dBW peak at 29

GHz). It is planar, scalable, compact and can scan ±70° with high XPD. The array consumes 169.2 W at P_{1dB} of 46 dBW at 29 GHz (280.5 W for P_{1dB} of 48 dBW at 27.5 GHz). Measured EVM is less than 2.3% for QPSK and 8-PSK modulation, with ACPR of less than -32 dBc, at P_{1dB} and up to 70° scan. This makes it suitable as a compact high efficiency SATCOM transmitter that is scalable to larger 4096-element phased-array and higher. To our knowledge, this is the largest wideband planar SATCOM Ka-band phased-array to-date with the highest EIRP and low AR across both scan and frequency.

Acknowledgment

The authors thank Renesas Electronics, for the beamformer chips, Keysight and Ansys for measurement equipment and design software, and Kyocera International, San Diego, for assembly.

Chapter 4, in part, is a reprint of the material as it appears in: K. K. Wei Low, S. Zihir, T. Kanar and G. M. Rebeiz, "A Reconfigurable Dual-Polarized 1024-Element Ka-Band SATCOM Transmit Phased-Array with Large Scan Volume and +48 dBW EIRP," presented at 2021 IEEE/MTT-S International Microwave Symposium (IMS), Atlanta, GA, USA, Jun. 10, 2021. The dissertation author was the primary investigator and author of this paper.

Chapter 4 is also, in full, has been submitted for publication of the material as it may appear in: K. K. Wei Low, S. Zihir, T. Kanar and G. M. Rebeiz, "A 27-31 GHz 1024-Element Ka-Band SATCOM Phased-Array Transmitter with 49.5-dBW Peak EIRP, 1-dB AR, and ±70° Beam Scanning," in *IEEE Transactions on Microwave Theory and Techniques*, submitted. The dissertation author was the primary investigator and author of this paper.

Chapter 5

A 17.7-20.2 GHz 1024-Element K-Band SATCOM Phased-Array Receiver with 8.1 dB/K G/T, $\pm 70^\circ$ Beam Scanning, and High Transmit Isolation

5.1 Introduction

There has been an increased interest in global high-speed internet connectivity, especially in low density areas (poorly served). Traditional internet service providers (ISPs) could not justify their financial interest serving those areas, and for users on a plane or ship, satellite communications (SATCOM) internet is the only solution available. This has led to a new space race by commercial companies to launch their space-based broadband connectivity with SATCOM systems such as Starlink, OneWeb, and Kuiper ([16]–[17]) with hopes of tapping this potentially lucrative market.

The new generation of SATCOM systems break away from traditional systems, which

operates a few large stationary satellites on geosynchronous orbit (GEO), by using many smaller satellites on the closer low earth orbit (LEO) and medium earth orbit (MEO). Doing so has the benefits of higher throughput, lower latency and true global coverage including coverage of the poles. Cost should, in theory, be lower since the new systems have lower user terminal cost and better economy of scale.

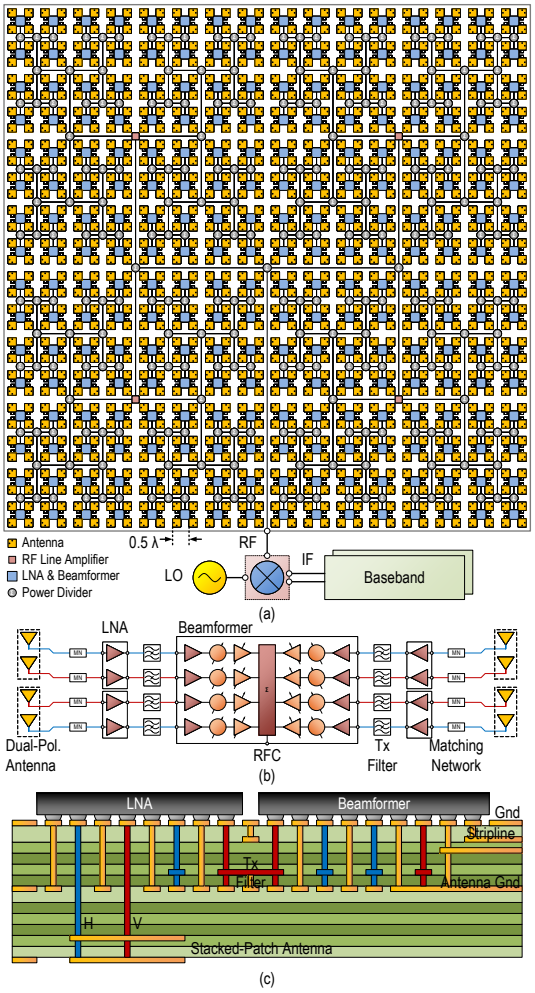

Figure 5.1: (a) Block diagram of the RF beamforming 1024-element SATCOM K-band phased-array receiver. (b) 2 x 2 dual-polarized antenna cell with eight-channel Rx beamformer, 4 dual-channel LNAs, matching network, and Tx-band filter. (c) PCB stackup with blind vias (3 set) and through vias.

However the new generation of LEO SATCOM requires the user terminal to track the satellite as it orbits around the earth, something which GEO-based system do not require for fixed ground systems. This necessitates either complex mechanical scanning units or active

electronically-scanned phased-arrays (AESA) (Fig. 5.1). With recent advances in commercial silicon beamforming chipsets, it is now feasible for the user terminals to be outfitted with AESA at relatively low cost. AESAs provide fast electronic beam-steering which is important for uninterrupted links between the user terminals and the moving satellites in LEO/MEO. Affordable phased-arrays also benefit current geostationary orbit (GEO) SATCOM systems especially for SATCOM-on-the-move systems [10]–[39].

In recent years, there has been several uplink (Ka-band) phased-array transmitters for SATCOM published ([13]–[38]), but only few downlink phased-array receivers for K-band SATCOM have been published ([40]–[41]). In this paper, an expanded companion of [18], a wideband reconfigurable dual-polarized (DP) 1024-element K-band SATCOM phased-array receiver is demonstrated with 8.1 dB/K G/T per polarization, low cross-polarization, $\pm 70^{\circ}$ beam scanning, and high transmit band isolation.

In Section II, we discuss the design of the phased-array from simulation to implementation. Measurements are presented in Section III and the paper ends with a comparison with the state of the art and a conclusion.

5.2 SATCOM Phased-Array Receiver Design

5.2.1 Architecture and Printed Circuit Board

The 1024-element phased-array receiver is based on an all RF beamforming architecture and its block diagram is shown in Fig. 5.1(a). Four dual-polarized (DP) antennas together with four dual-channel low noise amplifiers (LNAs) and an eight-channel receive (Rx) silicon beamformer (BF) form the 2x2 quad unit cell of the phased-array (Fig. 5.1(b)). 256 of these 2x2 quads, together with RF/digital line drivers and other circuity, are laid on a single printed circuit board (PCB) to form the 32x32 1024-element phased-array receiver.

The 8-channel beamformers enable individual amplitude and phase control for each

antenna polarization, and this allows the phased-array to receive all possible polarizations (linear, rotated linear, left- or right-hand circular polarization). Also, external dual-channel LNAs are used at the antenna ports to reduce the transmission loss from the antenna to the beamformer (Fig. 5.1(b)). For every 0.1 dB decrease in the line loss, the G/T improves by about 0.2 dB, and this results in about 1 dB improvement in G/T from the reduction of line loss alone. Finally, a high uplink (Ka-band transmit 27-31 GHz) isolation was achieved with antenna design and its low pass matching network. This ensures that nearby operating uplink terminals will not desense the phased-array receiver.

Panasonic Megtron6 with $\varepsilon_r = 3.26$ and $\tan\delta = 0.004$ was used for the PCB stackup (Fig. 5.1(c)). Layer M2 was used primarily for the stripline RF beamforming network (BFN) while parts of M1 and M5 were used for RF connection between antenna, LNA, and BF. Other layers were used for digital control, power and the antenna ground. The PCB is about 2 mm thick.

The phased-array is scalable by design and a larger phased-array, 4096-element for example, can quickly be constructed using an external power combiner ([29]–[20]) and without grating lobes.

5.2.2 Infinite Array Antenna Unit Cell

Microstrip patch antennas have been well studied in literature and it is well known that a single microstrip patch is narrowband with about 5% impedance bandwidth, while stacked-patch antennas has been shown to cover a wide fractional bandwidth (FBW) of up to 20% [21]–[22]. Together with its planar nature, this makes it suitable for a highly integrated phased-array covering the SATCOM K-band 17.7 to 21.2 GHz downlink frequency band (19%).

Fig. 5.2(a) presents the antenna unit cell of the phased-array. It is a stacked-patch probe-fed dual-polarized microstrip patch antenna with ground on M6. The antennas are matched to $50\,\Omega$ with a double-stub tuning network and connected to a dual-channel LNA on other side of the PCB (Fig. 5.2(b)). The antenna substrate thickness is $\lambda_0/15$ at 21 GHz.

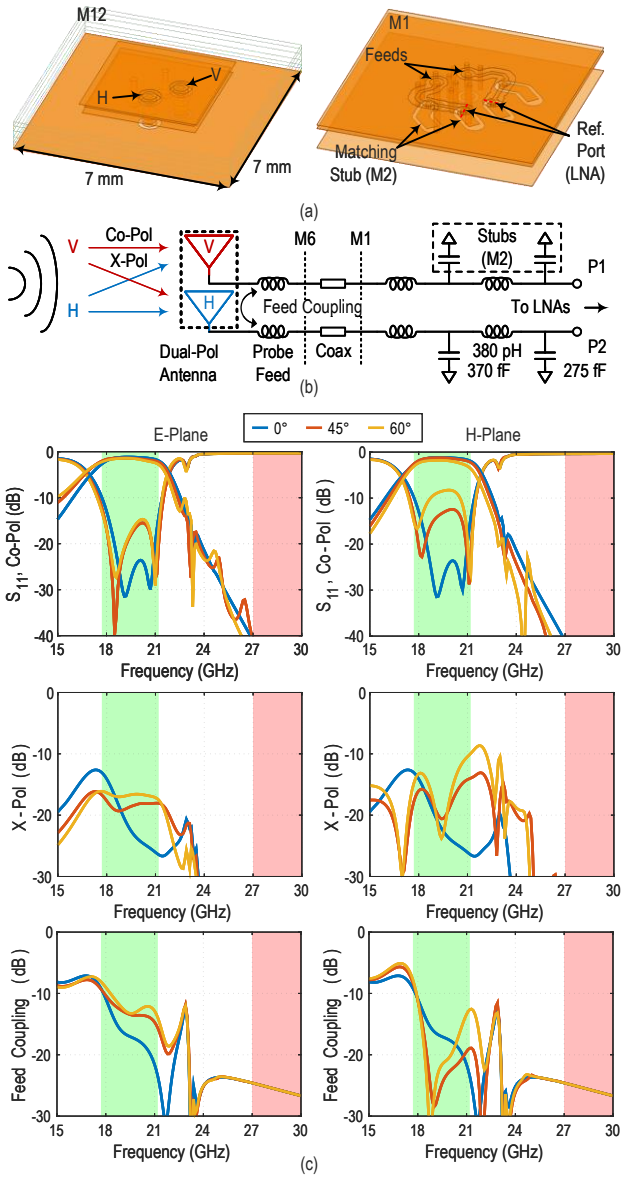

Figure 5.2: (a) Unit cell 3D layout of the dual-polarized probe-fed triple-stacked patch microstrip antenna with double stub matching network (some details hidden shown for clarity). (b) Equivalent circuit model of the antenna with matching network and (c) 3D FEM simulated performance in an infinite array.

The 7 mm (0.49λ) square lattice allows a grating lobe and scan blindness free scan range of ±77° up to 21.2 GHz [26]–[28], and results in a directivity of 4.14 dB per element at 19.5 GHz (mid-band)

$$D_{element} = 10log_{10}\left(\frac{4\pi D_x D_y}{\lambda^2}\right) = 4.14\,\text{dB}\,|_{19.5\,GHz} \tag{5.1}$$

where D_x, D_x are dimensions of the grid. The directivity of the 1024-element phased array is 34.2 dB with a 3-dB beamwidth of 3.5° under uniform illumination

$$D_{array} = D_{element} + 10log_{10}(1024) = 34.2\,\text{dB}\,|_{19.5\,GHz} \tag{5.2}$$

The unit cell, from the LNA reference input ports to the antenna including a wideband CLC matching network (MN) and coaxial transition, was simulated as an infinite array in a finite element method (FEM) simulator (HFSS), and the results are presented in Fig. 5.2(c). The antennas are well matched with S_{11} less than -13 dB and remains less than -9 dB for both H- and E-plane as the array scans to 60°. The cross-polar discrimination (XPD) is better than 14 dB on axis and remains more than 10.5 dB up to 60° scan. Coupling between the two polarization (due to un-shielded probes) remains less than -9 dB across scan.

The high XPD and good impedance match translates to a transmission of co-polarization of more than -1.1 dB at mid-band on axis and it does not degrade by more than 1.5 dB across scan and frequency. This is a simulated 79% radiation efficiency and includes antenna loss from the dielectric and ohmic effects, and from coaxial transition and MN.

The double-stub MN also acts as a second-order low-pass network to filter away the strong interference from nearby 27-31 GHz transmitters. An equivalent circuit of the MN is presented in Fig. 5.2(b) and it can be seen that the uplink Tx-band is suppressed by at least 40 dB across scan before it reaches the LNAs (Fig. 5.2(c)). Additional filtering of the Tx-band in the form of a single-stub stripline notch filter was included after the LNA and placed on M5 during the transition from the LNA to the beamformer (Fig. 5.3(a)).

Lastly, a technique of sequentially rotating the antenna feeds in a 2 x 2 antenna cell was implemented in this design. This is well covered in previous publications [29]–[20], [42] and further improves XPD as seen in Section III. Antenna D-plane simulated performance is approximately the average of H- and E-plane (not shown for brevity).

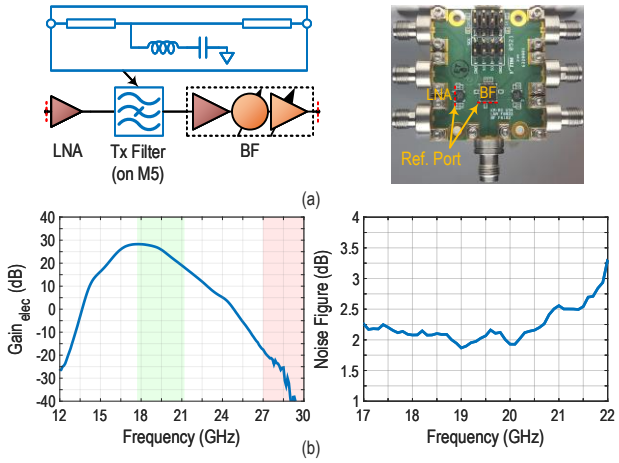

Figure 5.3: (a) LNA, stripline notch filter, beamformer channel, and the connectorized PCB. (b) Measured electronic gain and noise figure.

5.2.3 K-Band Receive Beamformer and LNA

The Renesas F6102 is a first-generation silicon eight channel receive (RX) beamformer (BF) chip designed for K-band SATCOM phased-array applications. The BF chip can be used with four dual-polarized or eight single-polarized antennas with its independently controllable channel amplitude and phase. The electronic gain and noise figure (NF) of F6102 is 9 dB and 5.5 dB, respectively. The F6102 BF comes in a 5 mm x 5 mm QFN package and is programmable via a high speed four wire serial-peripheral interface (SPI).

External LNAs (F6922) from Renesas were also used to lower system noise figure. The F6922 is a silicon dual-channel LNA chip with a gain and NF of 19 dB and 2 dB, respectively. The F6922 dual-channel LNA comes in a compact 2.7 mm x 2.7 mm BGA package.

Fig. 5.3(a) presents a block diagram (one channel only) and the connectorized PCB assembled for measurement of the LNA, filter, and BF channel. The combined LNA, filter, and BF chain provides 26 dB of electronic gain (includes ohmic loss of stripline transition and filter) and NF of 2.06 dB at 19.5 GHz (Fig. 5.3(b)). A separate measurement of the silicon LNA alone on a connectorized board (not shown) found that the NF and gain is 1.9 dB and 19.5 dB, respectively, at 19.5 GHz. This means that the de-embedded electronic gain and NF of the silicon

Table 5.1: RX SiGe Beamformer and LNA Summary

Parameter	Unit	F6102 BF	F6922 LNA
Frequency	GHz	17.5-21.5	17.7-21.2
No. of Channels	-	8	2
$Gain_{electronic}$	dB	9	19
Phase Shifter	bit	6	-
Phase Step	°	5.625	-
VGA Range	dB	30	-
VGA Step	dB	0.4	-
Noise Figure	dB	5.5	2
IP_{1dB}	dBm	-30	-20
Power/channel	mW	40	20
Supply Voltage	V	2.1-2.5	0.95-1.05

BF chip is 6.5 dB and 5.3 dB at 19.5 GHz, respectively. Note that the LNA/filter/BF gain and NF are 19 dB and 2.56 dB, respectively, at 21 GHz. This is due to the first-generation beamformer which shifted a bit down in frequency, thereby limiting the phased-array operating region to 20.2 GHz (for best performance). Table 5.1 summarizes key parameters of the F6102 BF and the F6922 LNA.

5.2.4 Tx-Band Rejection

The LNA and BF provides about 38 dB of Tx-band rejection at 27.5 GHz due to their narrowband response (centered at 19 GHz). An additional 5 to 15 dB of rejection is obtained when a single-section stripline notch filter is used with virtually no degradation to the NF since it is placed after the LNA. Together with 40 dB of rejection from the antenna response at 28 GHz, this means each element of the phased-array receiver will have at least 80 dB of Tx-band rejection.

This is an important point to consider in a simultaneous transmit and receive system where near-field coupling of transmit signal to the receiver may lead to receiver saturation. Assuming an average coupling ($C_{r/t}$) of -60 dB from a Tx antenna with a radiated power per element of 10

dBm (P_t), the power incident on the LNA input (P_{LNA}) will be

$$\begin{aligned} P_{LNA} &= P_t + G_t + C_{r/t} + A_t \\ &= 10\,\text{dBm} + 30\,\text{dB} - 60\,\text{dB} - 40\,\text{dB} \\ &= -60\,\text{dBm}\,|_{Tx-band} \end{aligned} \tag{5.3}$$

considering a combination of 1000 Tx antennas (G_t) in the vicinity and -40 dB Tx-band rejection of the receive antenna with its second-order low-pass matching network (A_t). The LNA will safely operate at its IP_{1dB} of -20 dBm without desense.

This also holds true for the power incident on the BF input port (P_{BF}) given by

$$\begin{aligned} P_{BF} &= P_{LNA} + G_{LNA} + G_{BSF} \\ &= -60\,\text{dBm} + 15\,\text{dB} - 8\,\text{dB} \\ &= -53\,\text{dBm}\,|_{Tx-band} \end{aligned} \tag{5.4}$$

where G_{LNA} and G_{BSF} are the gain of the LNA and stripline notch filter at the Tx-band, respectively. The BF will also safely operate at its IP_{1dB} of -30 dBm without desense.

5.2.5 Wilkinson Beamforming Network and RF Line Amplifier

The RF outputs of the 2x2 antenna elements are combined in the silicon beamformer and in the 256:1 corporate stripline beamforming network (BFN) on the PCB. The BFN implementation consists of printed Wilkinson power combiner and surface mount technology (SMT) resistors.

The Wilkinson power combiner equivalent circuit is presented in Fig. 5.4 and consists of printed stripline and 0201 sized SMT resistor soldered on M1. The simulated insertion loss of the Wilkinson power combiner was about 0.2 dB, with a return loss more than 20 dB, and an isolation more than 22 dB in the band of interest.

The BFN uses an equi-length H-topology and this leads to equal group delay from every

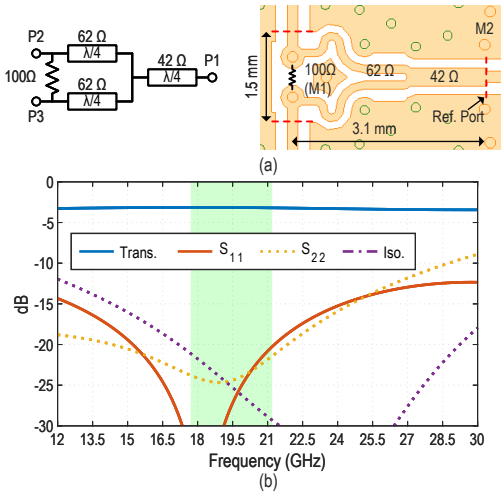

Figure 5.4: (a) Equivalent circuit of the stripline Wilkinson power combiner and layout. (b) 3D simulated response.

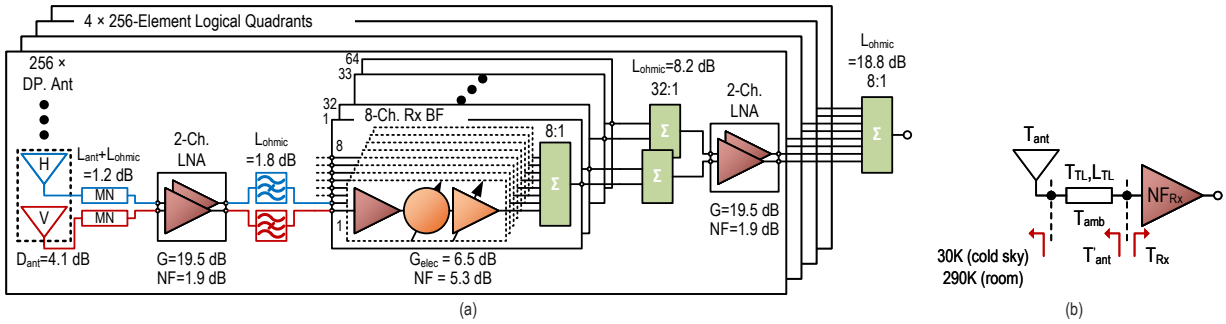

Figure 5.5: (a) RF system block diagram of the 1024-element phased-array receiver showing dual-channel LNAs used as RF line amplifiers in each 256-element quadrant. (b) Equivalent circuit model for G/T analysis.

element after combination. Equi-length topology simplifies calibration and reduces beam squint. Fig. 5.5(a) presents the RF system chain of the phased-array. It shows four additional F6922 LNAs are used in each 256-element quadrant as RF line amplifiers to overcome the Wilkinson network ohmic loss and preserve the low system noise figure of the phased-array.

5.2.6 Receiver Noise Figure and G/T

Fig. 5.5(b) presents the equivalent RF chain of the 1024-element phased-array. The electronic gain (G_{Rx}) of the phased-array at 19.5 GHz is

$$\begin{aligned} G_{Rx} &= \frac{P_{out}}{S_{inc} \cdot A_{inc}} \\ &= -1.2 + 19.5 - 1.8 + 6.5 - 8.2 + 19.5 - 18.8 \\ &= 15.5\,\text{dB} \end{aligned} \tag{5.5}$$

where P_{out} is the output power at the RF connector, S_{inc} is total power incident on the aperture, and A_{inc} is the area of the entire aperture. The phased-array system gain is high enough, and an external LNA/down-converter with a NF of 2-3 dB will result in virtually no degradation to the system performance.

The calculated phased-array receiver NF (NF_{Rx}) is

$$\begin{aligned} F_{Rx} &= F_{LNA} + \frac{F_{BSF} - 1}{G_{LNA}} + ... \\ &= 1.671\, or\, 2.23\,\text{dB}\,|_{19.5\,GHz} \end{aligned} \tag{5.6}$$

Since D_{array} is 34.2 dB at 19.5 GHz from (5.2), the array gain can be calculated for 1.2 dB antenna and MN ohmic loss as:

$$\begin{aligned} G_{array} &= D_{array} - L_{TL} \\ &= 34.2\,\text{dB} - 1.2\,\text{dB} \\ &= 33\,\text{dB}\,|_{19.5\,GHz} \end{aligned} \tag{5.7}$$

The array G/T can be calculated as:

$$\begin{aligned} G/T &= G_{array} - 10log_{10}(T_s) \\ &= 6.05\,\text{dB/K}\,|_{T_{ant}=290\,K} \\ &= 8.6\,\text{dB/K}\,|_{T_{ant}=30\,K} \end{aligned} \tag{5.8}$$

where T_s is the receiving system noise temperature. It consists of the effective antenna temperature (T'_{ant}) and the effective input noise temperature of the receiver (T_{Rx}).

$$\begin{aligned} T_s &= T'_{ant} + T_{Rx} \\ &= 497.1\,\text{K}\,|_{T_{ant}=290\,K} \\ &= 275.8\,\text{K}\,|_{T_{ant}=30\,K} \end{aligned} \tag{5.9}$$

T'_{ant} includes the temperature of the antenna (T_{ant}) and the MN with a loss of L_{TL}, connecting it to the receiver input (LNA).

$$T'_{ant} = T_{ant}/L_{TL} + T_{TL} \tag{5.10}$$

$$T_{TL} = T_{amb}(1 - 1/L_{TL}) \tag{5.11}$$

where T_{amb} is the average PCB temperature and assumed to be 30°C during operation. The calculated G/T at 19.5 GHz is 8.6 dB/K and 6.05 dB/K when the phased-array is facing the cold sky (T_{ant}=30K) and room temperature (T_{ant}=290K), respectively.

5.3 Calibration and Measurements

Fig. 5.6 presents the assembled phased-array receiver PCB. It contains 256 F6102 BF chips, 1020 F6922 LNA chips, driver chips, and measures 22.4 cm x 25.2 cm. The far-field range

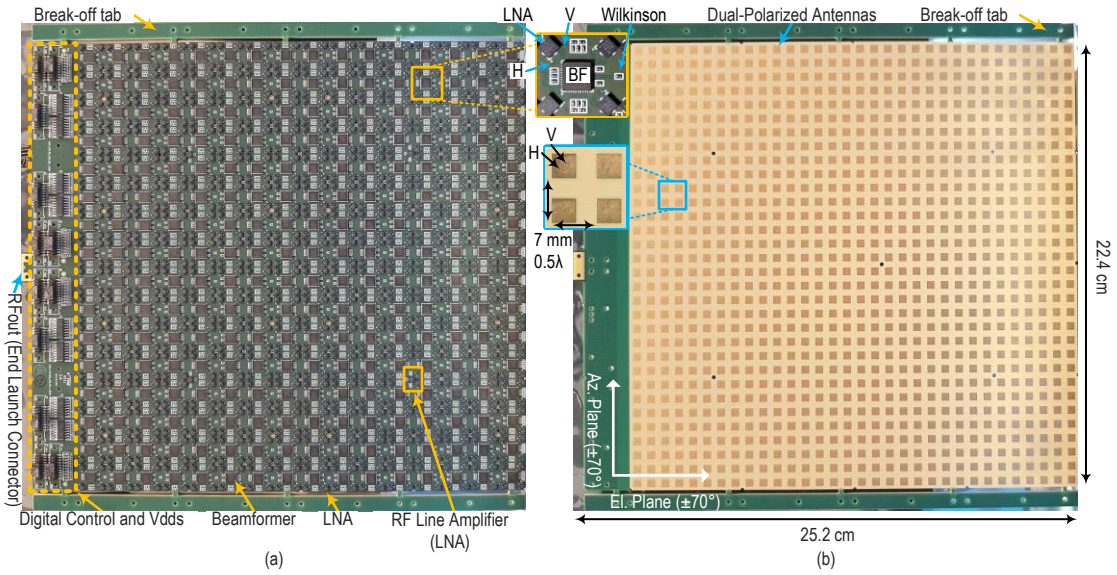

Figure 5.6: (a) Component side view and (b) antenna side view of the 1024-element phased-array showing sequential rotation of antennas in a 2x2 cell.

of the phased-array at 19.5 GHz is

$$\begin{aligned} R_{FF} &= \frac{2L^2}{\lambda} \\ &= 1.63\,\text{m}\,|_{256-quadrant} \\ &= 6.53\,\text{m}\,|_{1024-element} \end{aligned} \tag{5.12}$$

where L is the dimension of the antenna-under-test (AUT). The 1024-element phased-array was measured in an anechoic chamber with measurement range $R_{chamber}$ = 2.45 m which places the array in the Fresnel radiating near field region (Fig. 5.7). The phased-array antenna is effectively calibrated (focused) to the horn in this measurement setup.

Measurements were done using a elevation over azimuth motorized mount (MilliBox Positioner GIM03) with Keysight 4-port vector network analyzer (PNA-X N5247) and a dual-polarized horn (G_{horn} = 14 dB at 19.5 GHz, Eravant SAV-0632531431-SF-U3-QR). The phased-array is powered by Keysight power supplies and a single 80 mm fan was used to cool the PCB, keeping it under 55 °C. The phased-array consumes about 60 mW/channel and this is 122.9 W

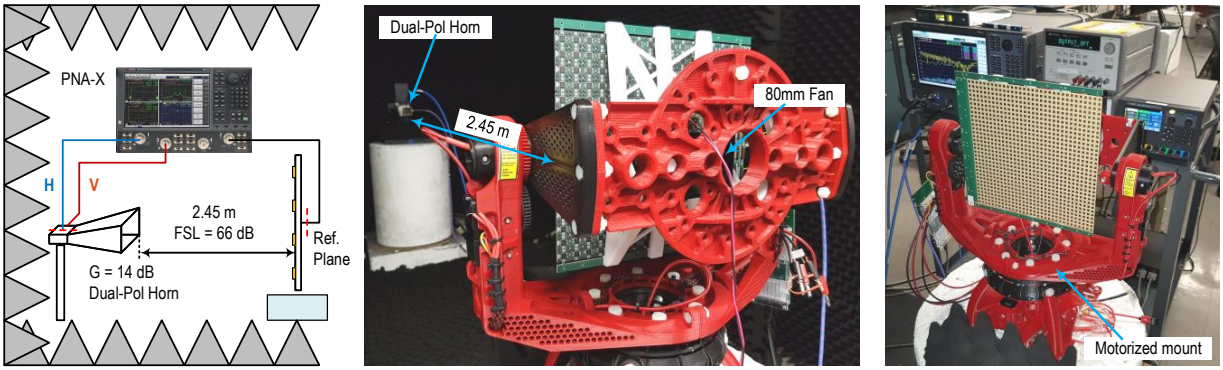

Figure 5.7: 1024-element SATCOM K-band phased-array receiver in an anechoic chamber.

for dual polarized operation (does not include 10 W consumed by the fan).

The phased-array could be operated without calibration but with reduced performance as care was taken to design the array to be as symmetrical as possible. A single calibration is all that is needed for most operation, as long as operating frequency does not differ from calibration frequency significantly. For this work, a single calibration was done at 19.5 GHz (mid-band) and on axis only.

Calibration of the phased-array was done using orthogonal-codes on a 256-element quadrant subarray level [43]. Orthogonal-code calibration has the advantage of higher signal-to-noise-and-leakage ratio (SNLR), accounts for active antenna impedance and operating temperature of the phased-array at the expense of longer calibration time.

The calibration procedure results in 0.72 and 0.63 dB root-mean-square (RMS) residual amplitude error, and 3.56 and 3.28° RMS residual phased error, for V-polarized and H-polarized quads respectively (Fig. 5.8). There are some outliers (mainly in the first quadrant) but, to a large extent, they do not affect the operation of large phased-arrays.

Fig. 5.9 presents the measured co- and cross-polarization phased-array frequency response of both the vertical and horizontal polarizations. The high attenuation of the Tx-band at about 70 dB shows the rejection ability of the 17.7-21.2 GHz antenna and is only limited by measurement noise floor. XPD levels of more than 25 dB were measured, due to the advantages of feed rotation,

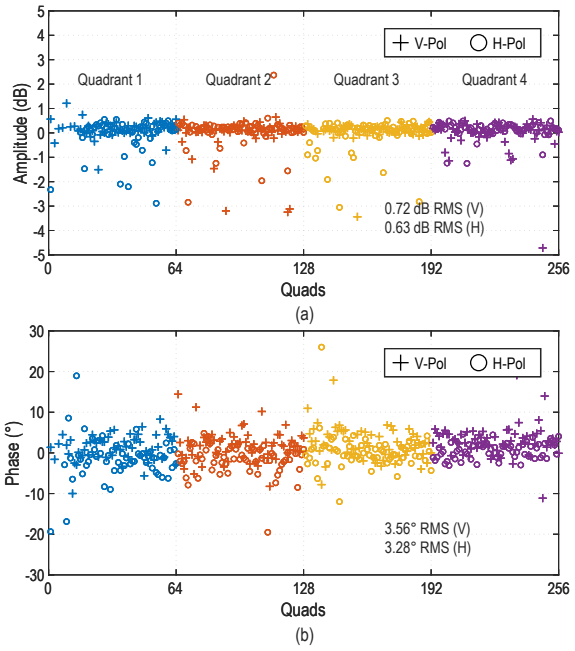

Figure 5.8: (a) Residual amplitude and (b) phase errors after calibration.

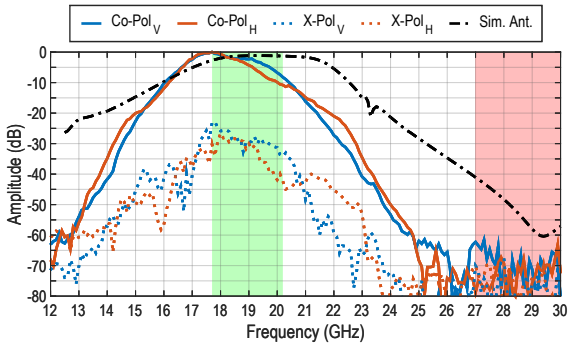

Figure 5.9: Measured linear co- and cross-pol frequency response of the 1024-element phased-array on axis (Green : Rx-band, Red : Tx-band).

and is limited by the dual-polarized horn.

The measured co-polarization response shows a 16-18 dB drop at 21.2 GHz compared to 18 GHz due to the combined response of the LNA and BF, and then another LNA in the chain. Also, the long Wilkinson combiner BFN has 1 dB more loss at 21.2 GHz than at 18 GHz. While the antenna and array design was meant to operate at 17.7-21.2 GHz, practical considerations related to the first-generation beamformer chip limited the operation to 20.2 GHz.

Dual-polarized phased-arrays have been shown to operate using left- or right-hand circular polarization (CP) in [13]–[18]. The phased-array receiver can be programmed to receive CP but only measured linear polarization (LP) will be presented due to setup limitations.

5.3.1 Patterns

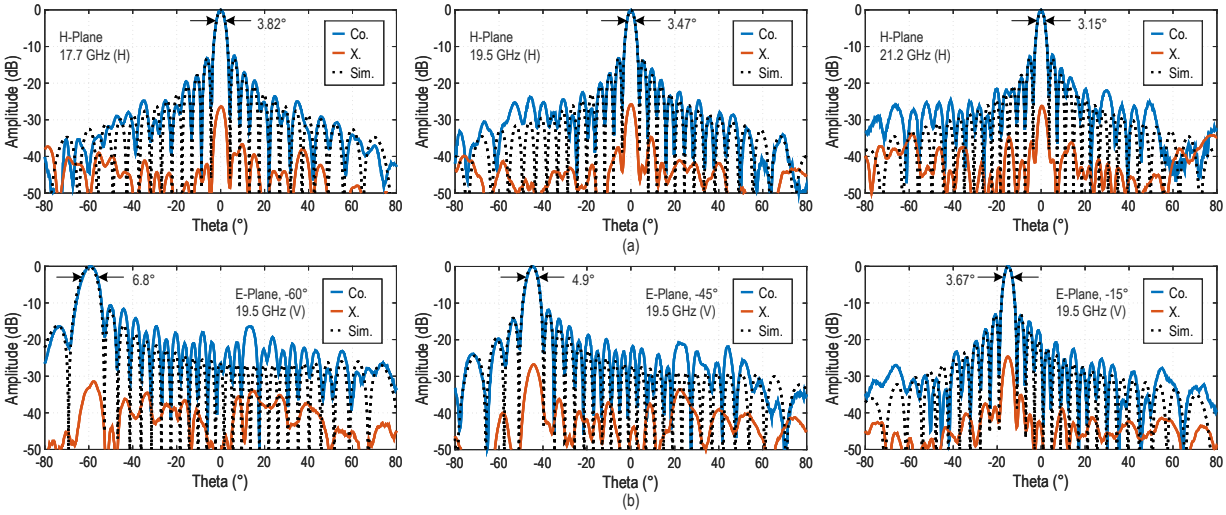

Figure 5.10: (a) Measured co- and cross-polarization for horizontal polarization at 17.7, 19.5, and 21.2 GHz (H-plane, El.). (b) Measured 19.5 GHz vertical co- and cross-polarization when scanned to -60°, -45°, and -15° (E-Plane, El.). The 1024-element phased-array was calibrated only once on axis at 19.5 GHz.

Fig. 5.10(a) presents measured co- and cross-polarization patterns at 17.7, 19.5, and 21.2 GHz with less than -11.5 dB sidelobe level (SLL) under uniform illumination. Note that the calibration was done only at 19.5 GHz and one can consider the 17.7-21.2 GHz on-axis patterns as an instantaneous bandwidth measurement. The beamwidths are 3.82°, 3.47°, and 3.15° on axis and the cross-polarization is under -25 dB. As the array scans to 60° (Fig. 5.10(b)) at 19.5 GHz, the beamwidth increases from 3.47° to 6.8° at 19.5 GHz. Cross-polarization remains under -25 dB (limited by setup) and no grating lobe is observed as expected.

There is good agreement between measured patterns versus calculated far-field patterns (dash lines) despite not being measured in the far-field. It also validates our calibration approach and shows that there is no beam-squint on axis.

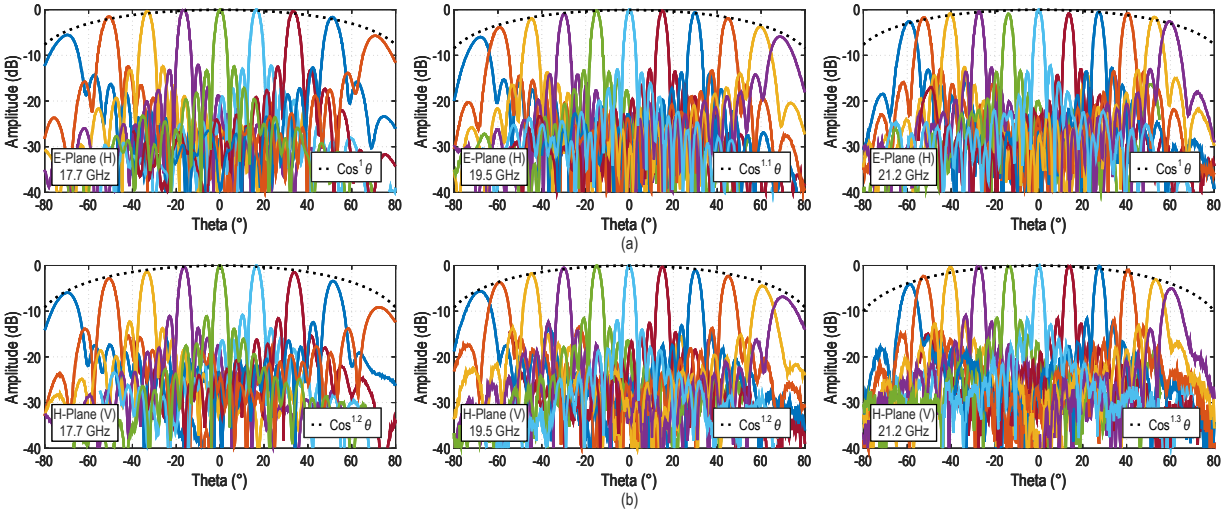

Figure 5.11: Measured scanned beams at 17.7, 19.5, and 21.2 GHz. (a) Horizontal polarization (E-plane, Az.). (b) Vertical polarization (H-plane, El.). Scanned beams along D-plane are similar to average of both Az. and El. but with less than -22 dB SLL (not shown).

Fig. 5.11 presents superimposed measured beam patterns for both the Azimuth (Az.) and Elevation (El.) planes as the phased-array scans to $\pm 70°$ at 19.5 GHz. No grating lobes were observed and the SLL remains lower than -11 dB. Lower SLL can be achieved with amplitude taper ([29]–[20]). Scanned pattern rolloff were found to be $cos^{1}(\theta)$, $cos^{1.1}(\theta)$, and $cos^{1}(\theta)$ along the E-plane and $cos^{1.2}(\theta)$, $cos^{1.2}(\theta)$, and $cos^{1.3}(\theta)$ along the H-plane for 17.7, 19.5, and 21.2 GHz, respectively. The patterns at 20.2 GHz are very similar to 19.5 GHz and are not shown. Also, patterns at 21.2 GHz are shown for antenna operation and not high G/T operation. Again note that the phase shift was applied only at 19.5 GHz, and the measured patterns at 17.7-21.2 GHz can be considered as an instantaneous bandwidth measurement. The beam squint effect is clearly evident (more scan angle at 17.7 GHz and less scan angle at 21.2 GHz).

Patterns along D-plane were similar to the average of Az. and El. planes but with better SLL (less than -22 dB under uniform illumination) as expected of rectangular aperture (not shown).

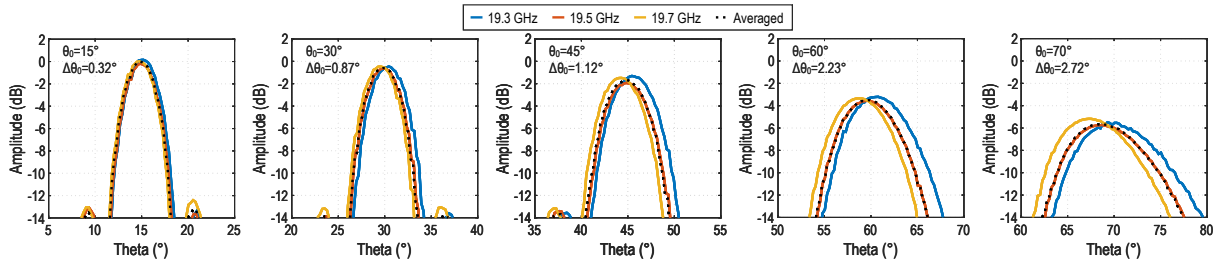

Figure 5.12: Measured beam-squint ($\Delta\theta_0$) from 19.3 to 19.7 GHz (400 MHz BW) when scanned to 15°, 30°, 45°, 60°, and 70°. No squinting occurs near axis and amplitudes are normalized to the axis at 19.5 GHz (not shown).

5.3.2 Beam-Squint

Fig. 5.12 presents the measured beam-squint ($\Delta\theta_0$) of the 1024-element phased-array for a 400 MHz waveform (centered at 19.5 GHz). K-band SATCOM channel bandwidths usually do not go beyond 400 MHz. A beam-squint of 0.32°, 0.87°, 1.12°, 2.23°, and 2.72° is obtained as the array scans to 70° at 400 MHz with a corresponding amplitude variation between the beams at f_{min} and f_{max} of less than 0.5 dB. Narrower signal bandwidth or using true time delay (TTD) will make beam-squint negligible and can be estimated as in [32].

There is also the question of inter-symbol interference (ISI) in large phased-arrays, but it can seen in [34] that ISI can be compensated using equalization during post processing in the digital domain.

5.3.3 G/T

The phased-array G/T is measured using the G/T measurement routine as outlined by Keysight and the PNA-X with NF option [44]–[45]. The G/T of the phased-array at room temperature (T_{ant} = T_0 = 290K) is found using:

$$G/T_{290K} = -NF_{setup} - 10log_{10}(T_0) + FSL - G_{horn} \tag{5.13}$$

where NF_{setup} is the noise figure of the measurement setup measured directly using the PNA-X (Fig. 5.7), G_{horn} is gain of the horn antenna and is 14 dB, and free space loss (FSL) is 66 dB at 19.5 GHz.

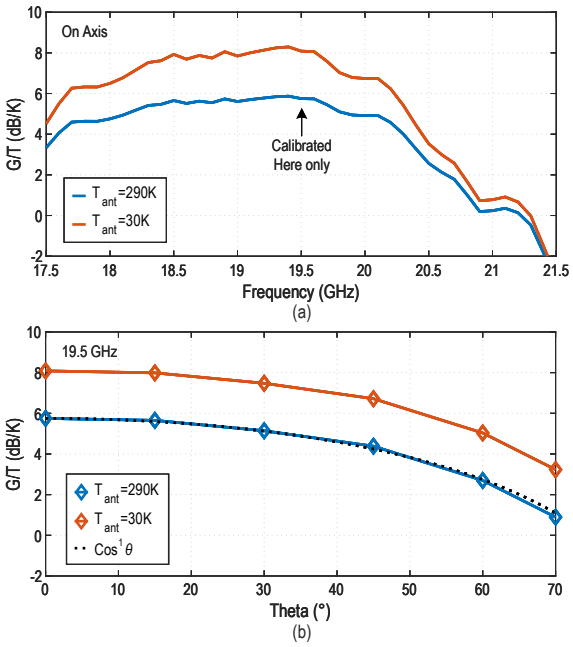

Figure 5.13: (a) Measured G/T on axis when the phased-array looks at room temperature, $T_{ant} = 290K$, and when it is looking at the cold sky ($T_{ant} = 30K$). (b) Measured G/T versus scan angle at 19.5 GHz.

The G/T is measured for the phased-array on axis and across scan at room temperature with T_{ant} = 290K (Fig. 5.13). The G/T when the phased-array is pointed at the cold sky (T_{ant} = 30K) is then calculated as

$$G/T_{30K} = G_{array} - 10log_{10}(T_{s,30K}) \tag{5.14}$$

where $T_{s,30K}$ is the receiving system noise temperature when the array is looking at the cold sky (T_{ant} = 30K) given by

$$T_{s,30K} = T_{s,290K} + \frac{30K - 290K}{L_{TL}} \tag{5.15}$$

and $T_{s,290K}$ is the receiving system noise temperature when looking at room temperature (T_{ant} = 290K) found using:

$$T_{s,290K} = 10^{(G_{array} - G/T_{290K})/10} \tag{5.16}$$

The measured G/T is 8.1 and 5.75 dB/K per polarization when T_{ant} = 30K and 290K, respectively, at 19.5 GHz on axis. This is close to the calculated values of 8.6 and 6.05 dB/K in (5.8). The G/T drops when the phased-array scans and closely follows a $cos^1(\theta)$ rolloff. The difference between the V and H polarization is ± 0.2 dB depending on frequency and the average between V and H is shown. This is expected since the array is focusing on the horn in the Fresnel zone and any misalignment versus frequency can result in slightly different values. Also, the G/T is lower than simulations because of the focusing effect to a small horn at $R_{FF}/4$. The entire wave is not captured by the horn (due to diffraction) and this results in a decrease in the measured G/T.

Table 5.2 provides a summary of the 1024-element phased-array receiver and compares it with state-of-the-art SATCOM phased-arrays.

5.4 Conclusion

This paper presented a low-profile planar, scalable, wideband 17.7-20.2 GHz, and dual-polarized 1024-element phased-array receiver with 8.1 dB/K G/T per polarization and high Tx-band isolation. To our knowledge, this is the largest wideband planar SATCOM K-band phased-array receiver to-date.

Table 5.2: Comparison with State-of-the-art SATCOM Phased-Arrays

Parameter	This Work	UCSD [29]	C-Com [15]
Frequency (GHz)	17.7 - 20.2	10.7 - 12.7	17.7 - 20.2
Fractional BW (%)	13.2	17.2	13.2
No. of Elements	32x32 (Rx)	16x16 (Rx)	16x16 (Rx)
Lattice Topology	Rectangular	Triangular	Rectangular
Lattice Spacing[1] (mm)	6.98 / 6.98	12.2 / 10.6	–
Polarization	Dual-Linear	Dual-Linear	Single-Circular
HPBW on Axis[1] (°)	3.47 / 3.47^{+}	7.6	6.5$^{\$}$
Scan Range[1] (°)	±70 / ±70	±70 / ±70	±70 / ±70
60° Scan Loss[1] (dB)	-3.3 / -3.3^{+}	-3.6	-3$^{\$}$
Sidelobe[2] (dB)	<-11 / <-22$^{@}$	<-12	<-10$^{\$}$
XPD on Axis[3,4] (dB)	>25*	>30	–
XPD vs Scan[3,5] (dB)	>25*	>19	–
G/T per pol.[3,4] (dB/K)	8.1	5	-1.0
P_{DC}[6] (W)	122.9	38.4$^{\#}$	–
$P_{DC}/Ch.$[7] (mW)	60	75$^{\#}$	168.75
Size (cm^2)	22.4 x 25.2	17 x 19.5	–

[1] Elevation/Azimuth or E-Plane/H-Plane [2] Uniform Illumination
[3] Linear-Polarization [4] Operating Frequency [5] Operating Scan Range
[6] Circular-Polarization or Dual-Polarization Mode
[7] P_{DC}/No. of Elements $^{+}$ Calibration Frequency $^{\$}$ From Graph
$^{@}$ D-Plane * Limited by setup $^{\#}$ Dual-Beam Mode

Acknowledgment

The authors thank Renesas Electronics, for the beamformer chips, Keysight and Ansys for measurement equipment and design software, and Kyocera International, San Diego, for assembly.

Chapter 5, in full, has been submitted for publication of the material as it may appear in: K. K. Wei Low, T. Kanar, S. Zihir and G. M. Rebeiz, "A 17.7-20.2 GHz 1024-Element K-Band SATCOM Phased-Array Receiver with 8.1 dB/K G/T, ±70° Beam Scanning, and High Transmit Isolation," in *IEEE Transactions on Microwave Theory and Techniques*, submitted. The dissertation author was the primary investigator and author of this paper.

Chapter 6

Conclusion and Future Work

6.1 Conclusion

This dissertation presented transmit and receive planar pahsed-arrays systems for Ka-band SATCOM ground and SOTM terminals. The arrays are all-silicon integrated on a single PCB and operate with high performance (EIRP or G/T).

In chapter 2, a 28-31 GHz Ka-band 256-element phased-array SATCOM transmitter with an EIRP of 34.5 dBW and more than 30 dB linear XPD was presented. The phased-array can scan to ±60° in the elevation plane with a 3-dB beamwidth of 7° and up to ±5° in the azimuth plane with 3.5° beamwidth. The compact size of (14 cm x 11.5 cm) makes it suitable for a low-cost Ka-band SATCOM ground terminal that is limited to 1-D scan.

In chapter 3, a 27-31 GHz 256-element Ka-band SATCOM transmit phased-array with embedded driver was presented. It demonstrates a measured 6.8° 3-dB beamwidth, +32 dBW (+62 dBm) EIRP on axis, greater than 25 dB cross-polar discrimination (XPD) and the ability to scan to ±70° in all planes. A compact size of 11.7 cm x 7.5 cm makes it suitable for Ka-band SATCOM and SOTM terminals.

In chapter 4, a 27-31 GHz 1024-element Ka-band SATCOM transmit (TX) phased-array

with embedded RF drivers was presented. It demonstrates a measured 3.5° half-power beamwidth (HPBW), 35 dB cross-polar discrimination (XPD), sub 1 dB axial ratio (AR), +49.5 dBW peak effective isotropic radiated power (EIRP) on axis and the ability to scan to ±70° in all planes without grating lobes and $cos^{1-1.1}(\theta)$ scan loss. Measured error vector magnitude (EVM) of less than 2.3% and adjacent channel power ratio (ACPR) of less than -32 dBc across all scan at P_{1dB} makes it suitable as a compact high efficiency SATCOM transmitter. The array aperture measures 14.9 cm by 14.9 cm and it is scalable to larger phased-arrays with 4096 and higher number of elements. To our knowledge, this represents the highest level of integration at millimeter-waves, and with the highest measured EIRP from a SATCOM phased-array. Note that the ability to operate the phased-array at P_{1dB} without sacrificing EVM and ACPR increases the array efficiency since a 2-3 dB backoff is not needed, and the phased-array can operate at P_{1dB} while still meeting SATCOM out-of-band requirements.

In chapter 5, a 17.7-20.2 GHz 1024-element K-band SATCOM receive (RX) phased-array was presented. It demonstrates a measured 3.47° half-power beamwidth (HPBW), more than 25 dB cross-polar discrimination (XPD), +8.1 dB/K gain to noise (G/T) per polarization, and has more than 80 dB Tx-band isolation. The phased-array is able to scan to $\pm 70°$ in all planes without grating lobes and $cos^{1-1.2}(\theta)$ scan loss. The array aperture measures 22.4 cm by 22.4 cm. To our knowledge, this is the largest SATCOM K-band phased-array to-date with the highest G/T and represents the highest level of integration at millimeter-waves.

6.2 Future Work

The Ka-band SATCOM phased-array systems presented in this dissertation may be expanded and improved in a few aspects :

1) For both Tx and Rx arrays, moving to a triangular lattice instead of a square/rectangular lattice will improve scan volume without introducing grating lobes. The increase in aperture area

means higher array aperture gain (16%) which in turn increases G/T for RX and increases EIRP for TX arrays. Thermals will also be improved. The only con of the lattice migration will be an increase in complexity of the layout.

2) For both Tx and Rx arrays, on-board transceiver integration will simplify connection to baseband equipment. Hybrid beamforming can also be realized if the transceiver is integrated on a subarray level, potentially adding subarray beams and correcting beam-squint in the digital domain.

3) For the Tx arrays, the power consumption will be decreased by using the next-generation beamformer chips from Renesas (available today). This will also improve the frequency response of the array, centering it at 29 GHz.

4) For the Tx arrays, Rx-band filtering should be added if the design allows to improve Tx-Rx co-existence. One method is using filtering antennas or filtering Wilkinson divider. Another method is to embed defected ground filters along the long beamforming network.

5) For the Rx arrays, power consumption and frequency response of the array can be improved by using the next-generation beamformer and LNA chips from Renesas (available today). This will center the frequency response at 19.5 GHz and also increase the operating frequency to 21.2 GHz. Using the next-generation LNA will also improve noise figure.

6) For the Rx arrays, two beams instead of one can be realized with use of beamformer chips with 2-beam capability from Renesas (available today). With 2 beams, the array can be used in monopulse mode for accurate angular detection and also velocity detection if FMCW signals are used. This will enable it to track the satellite or other flying objects without a-prior knowledge of movement/flight paths.

Bibliography

[1] S. Vaccaro, L. Diamond, D. Runyon, and M. Vigano, "Ka-band mobility terminals enabling new services," in *The 8th European Conference on Antennas and Propagation (EuCAP 2014)*, 2014, pp. 2617–2618.

[2] D. Wilcoxson, B. Sleight, J. O'Neill, and D. Chester, "Helicopter ku-band satcom on-the-move," in *MILCOM 2006 - 2006 IEEE Military Communications conference*, 2006, pp. 1–7.

[3] D. Wilcoxson, B. Sleight, D. Buchman, and R. Vandermeulen, "Ku-band satcom on-the move network," in *MILCOM 2005 - 2005 IEEE Military Communications Conference*, 2005, pp. 231–237 Vol. 1.

[4] N. Saponjic, F. Klefenz, F. Bongard, D. Llorens, A. Boulle, X. Aubry, A. Butler, F. Tiezzi, and S. Vaccaro, "Product concepts for land mobile satellite communication terminals in ku-/ka-band," in *2017 11th European Conference on Antennas and Propagation (EUCAP)*, 2017, pp. 1525–1529.

[5] A. H. Aljuhani, T. Kanar, S. Zihir, and G. M. Rebeiz, "A scalable dual-polarized 256-element ku-band phased-array satcom receiver with ±70° beam scanning," in *2018 IEEE/MTT-S International Microwave Symposium - IMS*, 2018, pp. 1203–1206.

[6] K. Kibaroglu, M. Sayginer, and G. M. Rebeiz, "A scalable 64-element 280hz phased-array transceiver with 50 dbm eirp and 8–12 gbps 5g link at 300 meters without any calibration," *2018 IEEE/MTT-S International Microwave Symposium - IMS*, pp. 496–498, 2018.

[7] G. M. Rebeiz and L. M. Paulsen, "Advances in satcom phased arrays using silicon technologies," in *2017 IEEE MTT-S International Microwave Symposium (IMS)*, 2017, pp. 1877–1879.

[8] K. Kibaroglu, M. Sayginer, and G. M. Rebeiz, "An ultra low-cost 32-element 28 ghz phased-array transceiver with 41 dbm eirp and 1.0–1.6 gbps 16-qam link at 300 meters," in *2017 IEEE Radio Frequency Integrated Circuits Symposium (RFIC)*, 2017, pp. 73–76.

[9] S. Borisov and A. Shishlov, "Antennas for satcom-on-the-move, review," in *2014 International Conference on Engineering and Telecommunication*, 2014, pp. 3–7.

[10] L. Paulsen, M. Livadaru, E. Dobbins, J. Wolf, J. West, A. Walker, V. Olen, J. Reyland, C. Olson, and G. Rebeiz, "Fabrication and measurement of a large, monolithic, PCB-based AESA," in *2016 IEEE International Symposium on Phased Array Systems and Technology (PAST)*, 2016, pp. 1–7.

[11] T. Takahashi, K. Yamamoto, T. Sakamoto, H. Suzuki, H. Arai, H. Joba, T. Okura, and H. Tsuji, "Wide-angle beam steering AESA with three-dimensional stacked PCB for Ka-band in-flight connectivity," in *2019 IEEE International Symposium on Phased Array System Technology (PAST)*, 2019, pp. 1–5.

[12] A. H. Aljuhani, T. Kanar, S. Zihir, and G. M. Rebeiz, "A scalable dual-polarized 256-element ku-band satcom phased-array transmitter with 36.5 dbw eirp per polarization," in *2018 48th European Microwave Conference (EuMC)*, 2018, pp. 938–941.

[13] K. K. Wei Low, A. Nafe, S. Zihir, T. Kanar, and G. M. Rebeiz, "A scalable circularly-polarized 256-element Ka-band phased-array SATCOM transmitter with ±60° beam scanning and 34.5 dBW EIRP," in *2019 IEEE MTT-S International Microwave Symposium (IMS)*, 2019, pp. 1064–1067.

[14] A. Nafe, M. Sayginer, K. Kibaroglu, and G. M. Rebeiz, "2x64 dual-polarized dual-beam single-aperture 28 GHz phased array with high cross-polarization rejection for 5G polarization MIMO," in *2019 IEEE MTT-S International Microwave Symposium (IMS)*, 2019, pp. 484–487.

[15] W. M. Abdel-Wahab, H. Al-Saedi, E. H. Mirza Alian, M. Raeis-Zadeh, A. Ehsandar, A. Palizban, N. Ghafarian, G. Chen, H. Gharaee, M. R. Nezhad-Ahmadi, and S. Safavi Naeini, "A modular architecture for wide scan angle phased array antenna for K/Ka mobile SATCOM," in *2019 IEEE MTT-S International Microwave Symposium (IMS)*, 2019, pp. 1076–1079.

[16] I. del Portillo Barrios, B. Cameron, and E. Crawley, "A technical comparison of three low earth orbit satellite constellation systems to provide global broadband," *Acta Astronautica*, vol. 159, 03 2019.

[17] S. Burleigh, T. Cola, S. Morosi, S. Jayousi, E. Cianca, and C. Fuchs, "From connectivity to advanced internet services: A comprehensive review of small satellites communications and networks," *Wireless Communications and Mobile Computing*, vol. 2019, pp. 1–17, 05 2019.

[18] K. K. Wei Low, S. Zihir, T. Kanar, and G. M. Rebeiz, "A reconfigurable dual-polarized 1024-element Ka-band SATCOM transmit phased-array with large scan volume and +48 dBW EIRP," in *2021 IEEE/MTT-S International Microwave Symposium (IMS)*, 2021.

[19] G. Gültepe, T. Kanar, S. Zihir, and G. M. Rebeiz, "A 1024-element Ku-band SATCOM phased-array transmitter with 45-dBW single-polarization EIRP," *IEEE Transactions on Microwave Theory and Techniques*, pp. 1–1, 2021.

[20] A. H. Aljuhani, T. Kanar, S. Zihir, and G. M. Rebeiz, "A 256-element Ku-band polarization agile SATCOM receive phased array with wide-angle scanning and high polarization purity," *IEEE Transactions on Microwave Theory and Techniques*, vol. 69, no. 5, pp. 2609–2628, 2021.

[21] D. Pozar, "Microstrip antennas," *Proceedings of the IEEE*, vol. 80, no. 1, pp. 79–91, 1992.

[22] K. Carver and J. Mink, "Microstrip antenna technology," *IEEE Transactions on Antennas and Propagation*, vol. 29, no. 1, pp. 2–24, 1981.

[23] R. Ramirez, F. De Flaviis, and N. Alexopoules, "Single-feed circularly polarized microstrip ring antenna and arrays," *IEEE Transactions on Antennas and Propagation*, vol. 48, no. 7, pp. 1040–1047, 2000.

[24] P. S. Hall, "Application of sequential feeding to wide bandwidth, circularly polarised microstrip patch arrays," vol. 136, no. 5, pp. 390–398, Oct 1989.

[25] J.-C. S. Chieh, E. Yeo, R. Farkouh, A. Castro, M. Kerber, R. B. Olsen, E. J. Merulla, and S. K. Sharma, "Development of flat panel active phased array antennas using 5G silicon RFICs at Ku- and Ka-bands," *IEEE Access*, vol. 8, pp. 192 669–192 681, 2020.

[26] A. Ishimaru and H.-S. Tuan, "Theory of frequency scanning of antennas," *IRE Transactions on Antennas and Propagation*, vol. 10, no. 2, pp. 144–150, 1962.

[27] A. Ishimaru, "Theory of unequally-spaced arrays," *IRE Transactions on Antennas and Propagation*, vol. 10, no. 6, pp. 691–702, 1962.

[28] D. Pozar and D. Schaubert, "Scan blindness in infinite phased arrays of printed dipoles," *IEEE Transactions on Antennas and Propagation*, vol. 32, no. 6, pp. 602–610, 1984.

[29] G. Gültepe and G. M. Rebeiz, "A 256-element dual-beam polarization-agile SATCOM Ku-band phased-array with 5-dB/K G/T," *IEEE Transactions on Microwave Theory and Techniques*, pp. 1–1, 2021.

[30] M. Mirmozafari, G. Zhang, C. Fulton, and R. J. Doviak, "Dual-polarization antennas with high isolation and polarization purity: A review and comparison of cross-coupling mechanisms," *IEEE Antennas and Propagation Magazine*, vol. 61, no. 1, pp. 50–63, 2019.

[31] C. Thakkar, A. Chakrabarti, S. Yamada, D. Choudhury, J. Jaussi, and B. Casper, "A 42.2-Gb/s 4.3-pJ/b 60-GHz digital transmitter with 12-b/symbol polarization MIMO," *IEEE Journal of Solid-State Circuits*, vol. 54, no. 12, pp. 3565–3576, 2019.

[32] S. K. Garakoui, E. A. M. Klumperink, B. Nauta, and F. E. van Vliet, "Phased-array antenna beam squinting related to frequency dependency of delay circuits," in *2011 41st European Microwave Conference*, 2011, pp. 1304–1307.

[33] A. H. Aljuhani, T. Kanar, S. Zihir, and G. M. Rebeiz, "A 256-element Ku-band polarization agile SATCOM transmit phased array with wide-scan angles, low cross polarization, deep nulls, and 36.5-dBW EIRP per polarization," *IEEE Transactions on Microwave Theory and Techniques*, vol. 69, no. 5, pp. 2594–2608, 2021.

[34] Z. Zhang, Y. Yin, and G. M. Rebeiz, "Intersymbol interference and equalization for large 5G phased arrays with wide scan angles," *IEEE Transactions on Microwave Theory and Techniques*, vol. 69, no. 3, pp. 1955–1964, 2021.

[35] Y. Yin, S. Zihir, T. Kanar, Q. Ma, H. Chung, L. Gao, and G. M. Rebeiz, "A 37–42-GHz 8 × 8 phased-array with 48–51-dBm EIRP, 64–QAM 30-Gb/s data rates, and EVM analysis versus channel RMS errors," *IEEE Transactions on Microwave Theory and Techniques*, vol. 68, no. 11, pp. 4753–4764, 2020.

[36] B. Rupakula, A. H. Aljuhani, and G. M. Rebeiz, "ACPR improvement in large phased arrays with complex modulated waveforms," *IEEE Transactions on Microwave Theory and Techniques*, vol. 68, no. 3, pp. 1045–1053, 2020.

[37] K. K. Wei Low, S. Zihir, T. Kanar, and G. M. Rebeiz, "A scalable switchable dual-polarized 256-element Ka-band SATCOM transmit phased-array with embedded RF driver and ±70° beam scanning," in *2020 IEEE/MTT-S International Microwave Symposium (IMS)*, 2020, pp. 821–824.

[38] X. Luo, J. Ouyang, Z.-H. Chen, Y. Yan, L. Han, Z. Wu, T. Yu, and K. Zheng, "A scalable Ka-band 1024-element transmit dual-circularly-polarized planar phased array for SATCOM application," *IEEE Access*, vol. 8, pp. 156 084–156 095, 2020.

[39] J. Navarro, "Ultra-small aperture terminals for SATCOM on-the-move applications," in *2017 IEEE MTT-S International Microwave Symposium (IMS)*, 2017, pp. 1152–1154.

[40] X. Luo, J. Ouyang, Z. Chen, L. Han, and W. Yan, "A low-profile 36-element K-band active phased array for ultra-small aperture application," *IEEE Access*, vol. 8, pp. 62 286–62 297, 2020.

[41] N. Ghaffarian, W. A. Wahab, A. Raeesi, E. A. Aminabad, A. Palizban, A. Ehsandar, M. Khaki, M.-R. Nezhad-Ahmadi, and S. Safavi-Naeini, "Characterization and calibration challenges of an K-band large-scale active phased-array antenna with a modular architecture," in *2020 50th European Microwave Conference (EuMC)*, 2021, pp. 1039–1042.

[42] A. Nafe, M. Sayginer, K. Kibaroglu, and G. M. Rebeiz, "2 x 64-element dual-polarized dual-beam single-aperture 28-GHz phased array with 2 x 30 Gb/s links for 5G polarization MIMO," *IEEE Transactions on Microwave Theory and Techniques*, vol. 68, no. 9, pp. 3872–3884, 2020.

[43] T. Phelps, Z. Zhang, and G. M. Rebeiz, "Phased-array calibration using orthogonal-codes with phase-shifter error correction and dynamic range requirements," *IEEE Transactions on Microwave Theory and Techniques*, 2021, submitted.

[44] R. Wansch, “A method for measuring G/T antenna performance in an anechoic chamber,” in *2009 3rd European Conference on Antennas and Propagation*, 2009, pp. 2212–2215.

[45] J. P. Dunsmore, “OTA G/T measurements of active phased array antenna noise using a vector network analyzer,” in *2020 94th ARFTG Microwave Measurement Symposium (ARFTG)*, 2020, pp. 1–4.